
First Hitting Diffusion Models for Generating Manifold, Graph and Categorical Data

Mao Ye,* Lemeng Wu, Qiang Liu
Department of Computer Science
The University of Texas at Austin

Abstract

We propose a family of First Hitting Diffusion Models (FHDM), deep generative models that generate data with a diffusion process that terminates at a random first hitting time. This yields an extension of the standard fixed-time diffusion models that terminate at a pre-specified deterministic time. Although standard diffusion models are designed for continuous unconstrained data, FHDM is naturally designed to learn distributions on continuous as well as a range of discrete and structure domains. Moreover, FHDM enables instance-dependent terminate time and accelerates the diffusion process to sample higher quality data with fewer diffusion steps. Technically, we train FHDM by maximum likelihood estimation on diffusion trajectories augmented from observed data with conditional first hitting processes (i.e., bridge) derived based on Doob’s h -transform, deviating from the commonly used time-reversal mechanism. We apply FHDM to generate data in various domains such as point cloud (general continuous distribution), climate and geographical events on earth (continuous distribution on the sphere), unweighted graphs (distribution of binary matrices), and segmentation maps of 2D images (high-dimensional categorical distribution). We observe considerable improvement compared with the state-of-the-art approaches in both quality and speed.

1 Introduction

Diffusion processes have become a powerful tool in various areas of machine learning (ML) and statistics. Traditionally, Langevin dynamics and Hamiltonian Monte Carlo have been foundations for learning and sampling from graphical models and energy-based models. Recently, denoising diffusion probabilistic models (DDPM) [18] and score matching with Langevin dynamics (SMLD) with its variants [41–43] have achieved the state-of-the-art results on data generation [13, 9, 30, 19].

Standard diffusion processes used in ML can be classified into two categories: 1) *infinite (or mixing) time* diffusion processes such as Langevin dynamics, which requires the process to run sufficiently long to converge to the *invariant distribution*, whose property is leveraged for the purpose of learning and inference; and 2) *fixed time diffusion* processes such as DDPM, SMLD, and Schrodinger bridges [11], which are designed to output the desirable results at a pre-fixed time. Although fixed-time diffusion has been show to surpass infinite time diffusion on both speed and quality, it still yield slow speed for modern applications due to the need of a pre-specified time and the incapability to adapt the time based on the difficulty of instances and problems. Moreover, standard diffusion models are naturally designed on \mathbb{R}^d , and can not work for discrete and structured data without special cares.

In this work, we study and explore a different *first hitting time* diffusion model that terminates at the first time as it hits a given domain, and leverages the distribution of the exit location (known as exit distribution, or harmonic measure [31]) as a tool for learning and inference. We provide the

*Corresponding author. Email: maoye21@utexas.edu

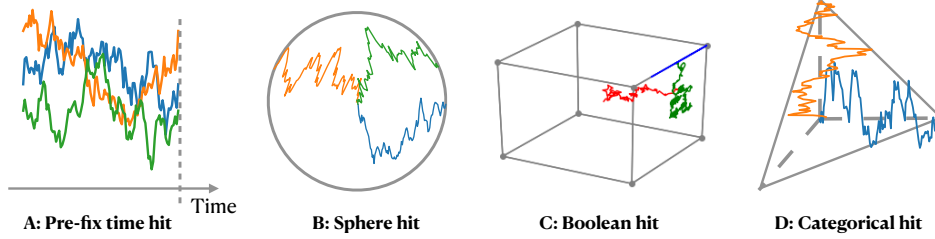


Figure 1: The four hitting schemes introduced in this paper. A: fixed-time hit, the process terminates at a fixed time; B: Sphere hit, hitting the boundary of a sphere from inside; C: Boolean hit, each coordinate terminates when it hits 0 or 1 and the whole process terminates when all of its coordinates terminate; D: Categorical hit, hitting the one-hot codes based on a conditioned process.

basic framework and tools for first hitting diffusion models. We leverage our framework to develop a general approach for learning deep generative models based on first hitting diffusion. This approach generalizes SMLD and its SDE extensions but can be attractively applied to a range of discrete and structured domains. This contrasts with the standard diffusion models, which are restricted to continuous \mathbb{R}^d data. In particular, we instantiate our framework to three cases, yielding new diffusion models for learning 1) spherical, 2) binary and 3) categorical data. In addition, the proposed diffusion model gives different instances adaptive arrival times and can generate high-quality samples using fewer diffusion steps. We discuss theoretical properties and fast implementation of our methods and demonstrate their practical efficiency in a suite of practical learning problems.

2 Main Framework

2.1 First Hitting Diffusion Processes

Let Π^* be a distribution of interest on a domain $\Omega \subset \mathbb{R}^d$. The goal is to construct a *first hitting stochastic process*, which starts from a point outside of Ω and returns a sample drawn from Π^* when it first hits set Ω . We start with introducing the new first hitting model.

Let $Z := \{Z_t : t \in [0, +\infty)\}$ be a continuous-time Markov process with probability law \mathbb{Q} taking value in a set V that contains Ω as a subset. Here \mathbb{Q} is a probability measure defined on the space of all continuous trajectories $C([0, +\infty), \mathbb{R}^d)$. We use \mathbb{Q}_t to denote the marginal distribution of Z_t at time t . We assume that the process is initialized from a point Z_0 outside of Ω . Denote by τ the *first hitting time* of Z_t on Ω , that is, $\tau = \inf_t \{t \geq 0 : Z_t \in \Omega\}$. We call that Z_t is absorbing to set Ω if

i) The process enters Ω in finite time almost surely when initialized from anywhere in V , that is, $\mathbb{Q}(\tau < +\infty \mid Z_0 = z) = 1, \forall z \in V$.

ii) The process stops to move once it arrives at Ω , that is, $\mathbb{Q}(Z_{t+s} = Z_t \mid Z_t \in \Omega) = 1, \forall s, t \geq 0$.

We define the *Poisson kernel* of \mathbb{Q} as the conditional distribution of Z_τ given $Z_t = z$, denoted by $\mathbb{Q}_\Omega(dx \mid Z_t = z) := \mathbb{Q}(Z_\tau = dx \mid Z_t = z)$. The marginal distribution of Z_τ , which we write as $\mathbb{Q}_\Omega(dx) = \mathbb{Q}(Z_\tau = dx)$, is called the *exit distribution*, or *harmonic measure*. Note that $\mathbb{Q}_\Omega(dx) = \int_V \mathbb{Q}_\Omega(dx \mid Z_0 = z) \mathbb{Q}_0(dz)$. The crux of our framework is to leverage the exit distribution \mathbb{Q}_Ω as a tool for statistical learning and inference, which is different from traditional frameworks that exploit the properties of the distributions at a fixed time or at convergence.

Example 2.1 (Sphere Hitting). *As shown in Figure 1-B, let $V = \{x \in \mathbb{R}^d : \|x\| \leq 1\}$ be the unit ball and $\Omega = S_d := \partial V$ the unit sphere. Let Z be a Brownian motion starting from $z \in V$ and stopped once it hits the boundary Ω . It is written as*

$$\mathbb{Q}^{S_d} : \quad dZ_t = \mathbb{I}(\|Z_t\| < 1) dW_t, \quad Z_0 \in V, \quad (1)$$

where W_t is a Wiener process; the indicator function $\mathbb{I}(\|Z_t\| < 1)$ sets the velocity to zero and hence stops the process once Z_t hits Ω . The Poisson kernel in this case is a textbook result:

$$\mathbb{Q}_\Omega^{S_d}(dx \mid Z_t = z) \propto \frac{1 - \|z\|^2}{\|x - z\|^d} \times \mu_\Omega(dz), \quad \text{where } \mu_\Omega \text{ is the surface measure on } \Omega = S_d. \quad (2)$$

Example 2.2 (Boolean Hitting). As shown in Figure 1-C, let $V = [0, 1]^d$ be the unit cube and $\Omega = B_d := \{0, 1\}^d$ the Boolean cube. Let Z be a Brownian motion starting from $Z_0 \in V$ and confined inside the cube V in the following way:

$$\mathbb{Q}^{B_d} : \quad dZ_{t,i} = \mathbb{I}(Z_{t,i} \in (0, 1))dW_{t,i}, \quad \forall i \in \{1, 2, \dots, d\},$$

where $Z_{t,i}$ is the i -th element of Z . Here, each coordinate $Z_{t,i}$ stops to move once it hits one of the end points (0 or 1). It can be viewed as a particle flying in a room that sticks on a wall once it hits it.

Proposition 2.3. The Poisson kernel of \mathbb{Q}^{B_d} is a simple product of Bernoulli distributions:

$$\mathbb{Q}_\Omega^{B_d}(x | Z_t = z) = \text{Ber}(x|z) := \prod_{i=1}^d \text{Ber}(x_i|z_i), \quad \text{where } \text{Ber}(x_i|z_i) = x_i z_i + (1 - x_i)(1 - z_i);$$

$\text{Ber}(x_i|z_i)$ is the likelihood function of observing $x_i \in \{0, 1\}$ under Bernoulli(z_i) with $z_i \in [0, 1]$.

Example 2.4 (Fixed Time Hitting). Our first hitting framework includes the more standard models with fixed terminal time. To see this, let $\bar{Z}_t = (t, Z_t)$ be a stochastic process Z_t with law \mathbb{Q} augmented with time t as one of its coordinates. Let $V = [0, t] \times \mathbb{R}^d$ and $\Omega = \{t\} \times \mathbb{R}^d$, where Ω is a vertical plane on the augmented space. Then the hitting time τ equals t deterministically, and the exit distribution equals the marginal distribution of Z_t at time t . See Figure 1-A, for illustration.

2.2 Diffusion Process Tools: Conditioning and h -transform

We introduce some basic tools for diffusion processes, including how to conduct conditioning, and exponential tilting (via h -transform) on diffusion processes. We apply these tools to the first hitting models we have. The readers can find related background in Oksendal [31], Särkkä and Solin [37].

Assume Z is a general Ito diffusion process in V that is absorbed to Ω , denoted as $\text{Ito}_\Omega(b, \sigma)$,

$$\mathbb{Q} \sim \text{Ito}_\Omega(b, \sigma) : \quad dZ_t = b_t(Z_t)dt + \sigma_t(Z_t)dW_t, \quad \forall t \in [0, +\infty), \quad Z_0 \sim \mathbb{Q}_0, \quad (3)$$

where $b_t(x) \in \mathbb{R}^d$ is the drift term and $\sigma_t(x) \in \mathbb{R}^{d \times d}$ is a positive definite diffusion matrix. We always assume that b and σ are sufficiently regular to yield a unique weak solution of (3).

Conditioning A step in our work is to find the distribution of the trajectories of a process \mathbb{Q} conditioned on a future event, e.g., the event of hitting a particular value x at exit, that is, $\{Z_\tau = x\}$. A notable result is that the conditioned diffusion processes are also diffusion processes. Given a point $x \in \Omega$ on the exit surface, the process of $\mathbb{Q}(\cdot | Z_\tau = x)$ can be shown to be the law of the following diffusion process [14, 37]:

$$\mathbb{Q}(\cdot | Z_\tau = x) : \quad dZ_t = (b_t(Z_t) + \sigma_t^2(Z_t) \nabla_{Z_t} \log q_\Omega(x | Z_t)) dt + \sigma_t(Z_t) dW_t, \quad Z_0 \sim \mu_{0|x}, \quad (4)$$

where $q_\Omega(x | z)$ is the density function of the Poisson kernel $\mathbb{Q}_\Omega(dx | Z_t = z)$ w.r.t. a reference measure μ_Ω on Ω , and σ^2 is the matrix square of σ , and the conditional initial distribution $\mu_{0|x} = \mathbb{Q}_0(\cdot | Z_\tau = x)$ is the posterior probability of Z_0 given $Z_\tau = x$.

Intuitively, the additional drift term $\nabla_{Z_t} \log p_\Omega(x | Z_t)$ plays the role of steering the process towards the target x , with an increasing magnitude as Z_t approaches Ω (because $P_\Omega(\cdot | Z_t = z)$ converges to a delta measure centered at x when z approaches Ω). This process is known as a diffusion *bridge*, because it is guaranteed to achieve $Z_\tau = x$ at the first hitting time with probability one.

Proposition 2.5. For \mathbb{Q}^{S_d} , the process conditioned on $Z_\tau = x \in S_d$ at exit is

$$\mathbb{Q}^{S_d}(\cdot | Z_\tau = x) : \quad dZ_t = \mathbb{I}(\|Z_t\| < 1) \left(\nabla_{Z_t} \log \frac{1 - \|Z_t\|^2}{\|x - Z_t\|^d} dt + dW_t \right). \quad (5)$$

Here the additional drift term (colored in blue) grows to infinity if $\|Z_t\| \rightarrow 1$ but $\|Z_t - x\|$ is large, and hence enforces that $Z_\tau = x$ when we exit the unit ball.

Proposition 2.6. For \mathbb{Q}^{B_d} , the process conditioned on $Z_\tau = x \in \{0, 1\}^d$ at exit is

$$\mathbb{Q}^{B_d}(\cdot | Z_\tau = x) : \quad dZ_{t,i} = \mathbb{I}(Z_{t,i} \in (0, 1)) \left(\frac{2x_i - 1}{x_i z_i + (1 - x_i)(1 - z_i)} dt + dW_{t,i} \right), \quad \forall i. \quad (6)$$

The additional drift term (colored in blue) enforces that $Z_{\tau,i} = x_i$ at the exit time as the drift would be infinite if z_i is still far from x_i when z_i is close to $\{0, 1\}$.

Proposition 2.7. *For the fixed time diffusion in Example 2.4, let \mathbb{Q}^T be the standard Brownian motion $dZ_t = dW_t$ stopped at a fixed time $t = T$, then \mathbb{Q} conditioned on $\mathbb{Q}^T(Z|Z_T = x)$ is*

$$\mathbb{Q}^T(\cdot|Z_T = x) : \quad dZ_t = \mathbb{I}(t \leq T) \left(\frac{Z_t - x}{T - t} dt + dW_t \right). \quad (7)$$

The additional drift (colored in blue) forces $Z_T = x$ as it grows to infinity if $Z_t \neq x$ while $t \rightarrow T$.

h-Transform Assume we want to modify the Markov process Z such that its exit distribution \mathbb{Q}_Ω matches the desirable target distribution Π^* . Doob’s *h-transform* [14] provides a simple general procedure to do so. Note that by disintegration theorem, we have $\mathbb{Q}(dZ) = \int \mathbb{Q}_\Omega(dx) \mathbb{Q}(dZ | Z_\tau = x)$, which factorizes \mathbb{Q} into the product of the exit distribution and the conditional process given a fixed exit location $Z_\tau = x$. To modify the exit distribution of \mathbb{Q} to Π^* , we can simply replace \mathbb{Q}_Ω with Π^* in the disintegration theorem, yielding

$$\mathbb{Q}^{\Pi^*}(dZ) := \int \Pi^*(dx) \mathbb{Q}(dZ | Z_\tau = x) = \pi^*(Z_\tau) \mathbb{Q}(dZ), \quad \text{with } \pi^*(Z_\tau) := \frac{d\Pi^*}{d\mathbb{Q}_\Omega}(Z_\tau), \quad (8)$$

where $\pi^* = \frac{d\Pi^*}{d\mathbb{Q}_\Omega}$ is the Radon–Nikodym derivative (or density ratio) between Π^* and \mathbb{Q}_Ω , and \mathbb{Q}^{Π^*} is called an *h-transform* of \mathbb{Q} . Intuitively, \mathbb{Q}^{Π^*} is the distribution of trajectories $Z \sim \mathbb{Q}(\cdot|Z_\tau = x)$ when the exit location x is randomly drawn from $x \sim \Pi^*$. We can also view $\pi^*(Z_\tau)$ as an importance score of each trajectory Z based on its terminal state Z_τ , and \mathbb{Q}^{Π^*} is obtained by reweighing (or tilting) the probability of each trajectory based on its score.

If \mathbb{Q} is a diffusion process, then \mathbb{Q}^{Π^*} is also a diffusion process. In addition, \mathbb{Q}^{Π^*} is the law of the following diffusion process:

$$\mathbb{Q}^{\Pi^*} : \quad dZ_t = \left(b_t(Z_t) + \sigma_t^2(Z_t) \nabla_z \log h_t^{\Pi^*}(Z_t) \right) dt + \sigma_t(Z_t) dW_t, \quad Z_0 \sim \mathbb{Q}_0^{\Pi^*} \quad (9)$$

where the initial distribution $\mathbb{Q}_0^{\Pi^*}$ and h^{Π^*} in the drift term are defined as

$$\mathbb{Q}_0^{\Pi^*}(dz) = \int_\Omega \pi^*(x) \mathbb{Q}(Z_\tau = dx, Z_0 = dz) \quad (10)$$

$$h_t^{\Pi^*}(z) = \mathbb{E}_\mathbb{Q}[\pi^*(Z_\tau) | Z_t = z] = \int_\Omega \pi^*(x) \mathbb{Q}(Z_\tau = dx | Z_t = z). \quad (11)$$

It is clear that h coincides with π^* on the boundary, that is, $h_{\pi^*}(x, t) = \pi^*(x)$ for all $x \in \Omega, t \geq 0$. The name of *h-transform* comes from the fact that h^{Π^*} is a (space-time) harmonic function w.r.t. \mathbb{Q} in the light of a mean value property: $h_t^{\Pi^*}(z) = \mathbb{E}_\mathbb{Q}[h_{t+s}^{\Pi^*}(Z_{t+s}) | Z_t = z], \forall s, t > 0$. \mathbb{Q}^{Π^*} yields a simple variational representation in terms of Kullback–Leibler (KL) divergence.

Proposition 2.8 (Variational Principle). *The \mathbb{Q}^{Π^*} in (8) yields*

$$\mathbb{Q}^{\Pi^*} = \arg \min_{\mathbb{P} \in \mathcal{P}(V, \Omega)} \left\{ \mathcal{KL}(\mathbb{P} || \mathbb{Q}) := \mathbb{E}_\mathbb{P} \left[\log \frac{d\mathbb{P}}{d\mathbb{Q}}(Z) \right], \quad \text{s.t. } \mathbb{P}_\Omega = \Pi^* \right\} \quad (12)$$

$$= \arg \min_{\mathbb{P} \in \mathcal{P}(V, \Omega)} \left\{ \mathcal{KL}(\mathbb{P} || \mathbb{Q}^{\Pi^*}) \equiv \mathcal{KL}(\mathbb{P} || \mathbb{Q}) - \mathbb{E}_\mathbb{P}[\log \pi^*(Z_\tau)] \right\}, \quad (13)$$

where $\mathcal{P}(V, \Omega)$ denotes the set of path measures on V that is absorbed to Ω .

Eq. (12) shows that \mathbb{Q}^{Π^*} is the distribution with Π^* as the exit distribution that has the minimum KL divergence with \mathbb{Q} . It can be viewed as a Schrodinger half bridge problem [e.g., 32], which enforces the constraint of $\mathbb{P}_T = \Pi^*$ at a fixed time T , rather than the first hitting time τ . Eq. (13) shows that the constraint can be turned into a penalty.

First Hitting Diffusion for Sampling The *h-transform* above readily provides a first hitting diffusion approach to approximate sampling from Π^* , assuming we can approximate the drift term h^{Π^*} . The Schrodinger-Follmer sampler [20] can be viewed as a special case of this approach with a fixed exit time. We leave further exploration to future works. See more discussion in Appendix A.3.

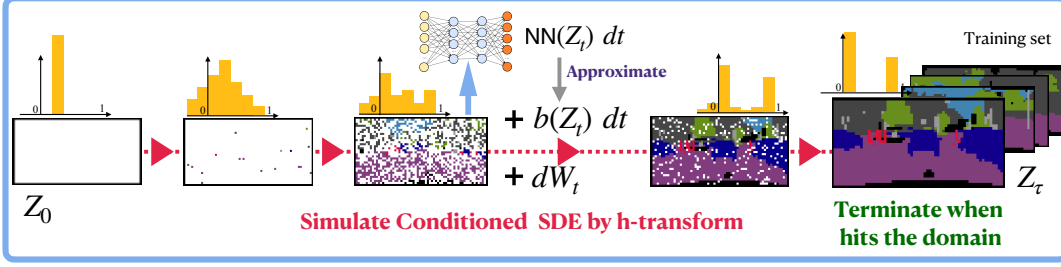


Figure 2: The training pipeline of FHD. Start from initial distribution, we use h-transform to simulate a conditioned SDE such that the process terminates at the desired destination data from training set at its hitting time. The network is trained to approximate the drift term ($b(Z_t)$), resulting a score-matching loss that is equivalent to the KL divergence.

Algorithm 1 Learning Generative Models by First Hitting Diffusion

Inputs & Goal: A data $\hat{\Pi} := \{x^{(i)}\}$ drawn from Π^* on Ω . A baseline process \mathbb{Q} and a model \mathbb{P}^θ that are absorbing to Ω . Want to find θ such that $\mathbb{P}_\Omega^\theta \approx \Pi^*$.

Training: Approximate $\hat{\theta} = \arg \min_\theta \mathcal{L}(\theta)$ by stochastic gradient descent with batches of data (approximately) drawn $Z \sim \mathbb{Q}(\cdot | Z_\tau = x)$ and $x \sim \hat{\Pi}$.

Inference: Simulate $\mathbb{P}^{\hat{\theta}}$.

2.3 Learning First Hitting Diffusion Models

We illustrate the learning pipeline of our First Hitting Diffusion Models (FHD) in Figure 2. Assume Π^* is unknown and we observe it through an i.i.d. sample $\{x^{(i)}\}_{i=1}^n$ drawn from Π^* . We want to fit the data with a parametric diffusion process $\text{It}_{\Omega}(s_\theta, \sigma)$ in V that is absorbing to Ω ,

$$\mathbb{P}^\theta : \quad dZ_t = s_t^\theta(Z_t)dt + \sigma_t(Z_t)dW_t, \quad Z_0 \sim \mathbb{P}_0^\theta, \quad (14)$$

such that the exit distribution \mathbb{P}_Ω^θ matches the unknown Π^* . Here $s_t^\theta(z)$ is a deep neural network with input (z, t) and parameters θ . We should design s^θ and σ properly to ensure the absorbing property. The standard approach to estimate Π^* is maximum likelihood estimation, which can be viewed as approximately solving $\min_\theta \mathcal{KL}(\Pi^* \parallel \mathbb{P}_\Omega^\theta)$. However, calculating the likelihood of the exit distribution \mathbb{P}_Ω^θ of a general diffusion process is computationally intractable. To address this problem, we fix \mathbb{Q} as a “prior” process, and augment the data distribution Π^* to the h-transform \mathbb{Q}^{Π^*} , whose exit distribution $\mathbb{Q}_\Omega^{\Pi^*}$ matches Π^* by definition. Note that we can draw i.i.d. sample from \mathbb{Q}^{Π^*} in a “backward” way: first drawing an exit location $x \sim \Pi^*$ from the data, and then draw the trajectory Z from $\mathbb{Q}(\cdot | Z_\tau = x)$ with the fixed exit point. To train a generative model, we train \mathbb{P}^θ to fit it with the data drawn from \mathbb{Q}^{Π^*} by maximum likelihood estimation:

$$\min_\theta \left\{ \mathcal{L}(\theta) := \mathcal{KL}(\mathbb{Q}^{\Pi^*} \parallel \mathbb{P}^\theta) \equiv -\mathbb{E}_{Z \sim \mathbb{Q}^{\Pi^*}} [\log p^\theta(Z)] + \text{const}, \right\},$$

where $p^\theta = \frac{d\mathbb{P}^\theta}{d\mathbb{Q}^{\Pi^*}}$ is Radon–Nikodym density function of \mathbb{P}^θ relative to \mathbb{Q}^{Π^*} . By the chain rule of KL divergence in (20) in Appendix A.9, we have $\mathcal{KL}(\Pi^* \parallel \mathbb{P}_\Omega^\theta) \leq \mathcal{KL}(\mathbb{Q}^{\Pi^*} \parallel \mathbb{P}^\theta)$. Therefore, if minimizing the KL divergence allows us to achieve $\mathbb{P}^\theta \approx \mathbb{Q}^{\Pi^*}$, we should also have $\mathbb{P}_\Omega^\theta \approx \mathbb{Q}_\Omega^{\Pi^*} = \Pi^*$.

Using Girsanov theorem [24], we can calculate the density function p^θ and hence the loss function.

Proposition 2.9. Assume \mathbb{Q} in (3), and \mathbb{P}^θ in (14) are absorbing to Ω . We have

$$\mathcal{L}(\theta) = \frac{1}{2} \mathbb{E}_{\mathbb{Q}^{\Pi^*}} \left[\int_0^\tau \|\sigma_t(Z_t)^{-1} (s_t^\theta(Z_t) - b_t(Z_t | Z_\tau))\|^2 dt - \log p_0^\theta(Z_0) \right] + \text{const}, \quad (15)$$

where $b_t(z|x) := b_t(z) + \sigma_t^2(z) \nabla_z \log p_\Omega(x|z)$ is the drift of the conditioned process $\mathbb{Q}(\cdot | Z_\tau = x)$ in (4), and p_0^θ is the probability density function of the initial distribution \mathbb{P}_0^θ . In addition, θ^* achieves the global minimum of $\mathcal{L}(\theta)$ if

$$s_t^{\theta^*}(z) = \mathbb{E}_{Z \sim \mathbb{Q}^{\Pi^*}} [b_t(z | Z_\tau) | Z_t = z], \quad \mathbb{P}_0^{\theta^*} = \mathbb{Q}_0^{\Pi^*} = \mathbb{E}_{x \sim \Pi^*} [\mathbb{Q}_0^x(\cdot)].$$

Therefore, the optimal drift term $s_t^{\theta^*}$ should match the conditional expectation of $b_t(z|x)$ with $x \sim \mathbb{Q}_\Omega(\cdot|Z_t = z)$, which coincides with the drift of \mathbb{Q}^{Π^*} in (9). The initial distribution of \mathbb{P}^θ should obviously match the initial distribution of \mathbb{Q}^{Π^*} . In practice, we recommend eliminating the need of estimating \mathbb{P}^{θ_0} by starting \mathbb{Q} from a deterministic point $Z_0 = z_0$, in which case \mathbb{P}^θ should initialize from the same deterministic point. See Algorithm 1.

Learning Spherical Hitting Models Take $\mathbb{Q} = \mathbb{Q}^{S_d}$ in Example 2.1, we get a method for learning generative models for data on the unit sphere. We set the model to be $dZ_t = \mathbb{I}(\|Z_t\| < 1)(f_t^\theta(Z_t)dt + dW_t)$ to ensure that it is absorbing to S_d . The loss function is

$$\mathcal{L}(\theta) = \frac{1}{2} \mathbb{E}_{\substack{x \sim \Pi^* \\ Z \sim \mathbb{Q}^x}} \left[\int_0^\tau \left\| f_t^\theta(Z_t) - \nabla_{Z_t} \log \frac{1 - \|Z_t\|^2}{\|x - Z_t\|^d} \right\|^2 dt - \log p_0^\theta(Z_0) \right] + \text{const.}$$

Learning Boolean Hitting Models Taking $\mathbb{Q} = \mathbb{Q}^{B_d}$ as in Example 2.2 provides an approach to learning diffusion generative models for binary variables. We set the model \mathbb{P}^θ to be $dZ_t = \mathbb{I}(Z_t \in (0, 1)) \circ (f_t^\theta dt + dW_t)$ to ensure that \mathbb{P}^θ is absorbing to B_d like \mathbb{Q}^{B_d} , where \circ denotes element-wise multiplication. The loss function is

$$\mathcal{L}(\theta) = \frac{1}{2} \mathbb{E}_{\substack{x \sim \Pi^* \\ Z \sim \mathbb{Q}^x}} \left[\int_0^\tau \left\| \mathbb{I}(Z_t \in (0, 1)) \circ (f_t^\theta(Z_t) - \nabla_{Z_t} \log \text{Ber}(Z_t|x)) \right\|^2 dt - \log p_0^\theta(Z_0) \right] + \text{const.}$$

Learning Fixed Time Diffusion Models Following the fixed time setting in Example 2.4, we can recover the standard fixed time diffusion models for continuous data, such as SMLD and DDPM. In particular, a natural choice is to set \mathbb{Q} to be an O-U process $dZ_t = \alpha_t Z_t dt + \sigma_t dW_t$ initialized from $Z_0 \sim \mathcal{N}(0, v_0)$ where $\sigma_t \geq 0, v_0 > 0$. We show in Appendix A.4 that SMLD ($\alpha_t = 0$) and DDPM ($\alpha_t > 0$) is recovered as the limit case when $v_0 \rightarrow +\infty$.

2.3.1 Learning Categorical Generative Models

In addition to the boolean hitting model, we provide here a first hitting framework for learning categorical data. In this case, the data domain Ω is $C_{d,m} = \{e_1, \dots, e_d\}^m$, where $e_i = [0, \dots, 1, \dots, 0]$ is the i -th one-hot (or basis) vector in \mathbb{R}^d , so the data is a m -dimensional and d -categorical.

It is less straightforward to construct a first hitting diffusion process that is absorbing to $C_{d,m}$. We leverage the conditioning technique to achieve this. We explain the idea with $m = 1$, of which the general case is a direct product. The key observation is that the one-hot vectors $C_{d,1}$ is a subset of the boolean cube $B_d = \{0, 1\}^d$. Hence, by definition, the conditioned process $\mathbb{Q}^{C_{d,1}} := \mathbb{Q}^{B_d}(\cdot|Z_\tau \in C_{d,1})$ exits at $C_{d,1}$ from the inside of B_d . Using the method of h -transforms [14, 37], $\mathbb{Q}^\Omega := \mathbb{Q}^{B_d}(\cdot|Z_\tau \in \Omega)$ for any $\Omega \subset B_d$ is the law of

$$dZ_t = \mathbb{I}(Z_t \in (0, 1)) \circ (\nabla_z \log \text{Ber}(\Omega | Z_t) dt + dW_t), \quad \text{Ber}(\Omega | z) := \sum_{e \in \Omega} \text{Ber}(e | z).$$

Another challenge is to construct a parametric family of \mathbb{P}^θ that is absorbing to $C_{d,m}$, regardless of the value of θ . The result below shows that this can be done by simply adding on top of \mathbb{Q}^Ω any bounded neural network drift term.

Proposition 2.10. *Let $V = [0, 1]^d$ and Ω is any subset of $B_d = \{0, 1\}^d$. Assume $f_t^\theta(z)$ is any bounded measurable function. Then the following process is guaranteed to hit Ω when it exits V :*

$$dZ_t = \mathbb{I}(Z_t \in (0, 1)) \circ (f_t^\theta(Z_t) + \nabla_z \log \text{Ber}(\Omega | Z_t) dt + dW_t), \quad Z_0 \in (0, 1)^d.$$

See Appendix A.1 for the summary of the algorithm for learning categorical data.

2.3.2 Fast Sampling of Bridges

One main step in calculating the loss $\mathcal{L}(\theta)$ is to draw trajectory Z from the bridge $\mathbb{Q}^x = \mathbb{Q}(\cdot | Z_\tau = x)$. This can be achieved by simulating the bridge processes using Euler–Maruyama method. This is not computationally costly because it is the simulation of elementary SDEs and does not involve deep neural networks. However, it does cause a slow down in the training algorithm if the data x is very high dimensional and the data size is very large.

To speed up the training, we propose a fast algorithm for simulating bridges by exploiting the symmetry when we initialize from a point z_0 (e.g., the center of sphere) around which Ω and \mathbb{Q} are rotational symmetric. The idea is simple: we simulate the *unconditioned* process \mathbb{Q} to get a trajectory Z that exits at any point. Then, to obtain the conditional process $\mathbb{Q}(\cdot|Z_\tau = x)$, we simply rotate the trajectory Z such that the exit point Z_τ is transformed from the original one to x . An advantage is that we can pre-simulate a large number of trajectories before training and only need to apply the rotation operator to get specific conditioned processes during training. Figure 3 gives an illustration using the example of sphere hit. The idea can be applied similarly for other types of hitting.

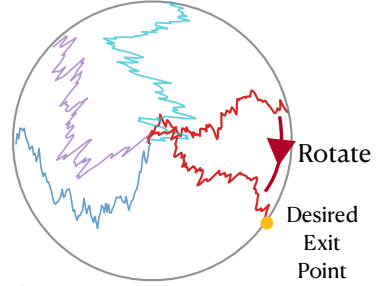


Figure 3: To sample a conditioned process, we can pick up a trajectory of unconditioned process and rotate it so that it exits at a given point.

Proposition 2.11. *Assume Z with law \mathbb{Q} initialized from $z_0 \in \mathbb{R}^d$ is absorbing to Ω . For $x, x' \in \Omega$, let $\text{rot}_{x' \rightarrow x}$ be the rotation operator around z_0 that transforms x' to x (hence $\text{rot}_{x' \rightarrow x}(x') = x$). Assume that Ω and \mathbb{Q} are rotation invariant around z_0 in that $\text{rot}_{x', x}(\Omega) = \Omega$ and $\text{rot}_{x', x}(Z) \sim \mathbb{Q}$ when $Z \sim \mathbb{Q}$ for any $x', x \in \Omega$. Then if $Z \sim \mathbb{Q}$, we get $Z' = \text{rot}_{Z_\tau \rightarrow x}(Z)$, a sample drawn from $\mathbb{Q}(\cdot|Z_\tau = x)$.*

Such a fast sampling approach is applicable for all the categorical, sphere and binary distributions.

2.4 Discretization Error

In practice, the Euler-Maruyama method is applied to discretize the process. Analyzing the discretization error of a random hitting process is more difficult than that of a fixed-time process. In a fixed-time process, both discretized and continuous processes terminate at the same time, making the coupling tricks applicable for analyzing the discretization error based on the ℓ_2 Wasserstein distance. Standard analysis under Lipschitz continuity assumption of the drifts gives $O(\Delta)$ error rate where Δ is the discretization step size [37]. In comparison, the key challenge of analyzing the FHDM is that the discretized and continuous processes may not terminate at the same time, and thus we need to bound the probability of the difference of the hitting time distribution in the analysis. Besides, in practice, we might also apply some time truncation tricks in order to have a bounded waiting time for generating. In Appendix A.8, we provide a full analysis and show that FHDM also yields $O(\Delta)$ discretization error asymptotically.

3 Related Work

Diffusion Generative Model on Different Domains Diffusion generative model has been demonstrated to be powerful in generation of general continuous data such as image [40, 41, 18, 42, 43, 13], point cloud shape [7, 26, 49] and audio [9, 22]. Recently, diffusion generative model has also been extended to learn to generate data on special domains such graph [30], segmentation map [19], text [19] and manifold data [12]. Such a generalization of diffusion model is usually case-by-case and is based on applying constraints to ensure the data remains in the desired domain during the diffusion process [19, 12] or use heuristic approximation to round the data into the discrete space [30]. Our FHDM gives a unified framework for generating data on special domain via a completely new mechanism of first hitting.

Theoretical Framework on Diffusion Process Most existing diffusion models are based on the framework of time-reversing [43] in which the generation (i.e. denoising) process is learned based on its time-reversed stochastic differential equation trajectory that can be simulated easily, ignoring the mismatch of the initial distribution. In comparison, our framework is conceptually simpler and is only based on a forward process, in which the learning is based on conditioned stochastic differential equations (i.e., bridge) that can be simulated via h -transform. A similar framework is independently explored in [34] but our method is more general and exploits the idea of first hitting. Schrodinger bridges is another well studied framework of diffusion model [46, 11, 34, 10]. However, using Schrodinger bridges usually require expensive forward-backward algorithms. It is also unknown whether or how Schrodinger bridges can be applied for generating data in special domains.

Model	Airplane				Chair			
	MMD↓	COV↑	1-NNA↓	JSD↓	MMD↓	COV↑	1-NNA↓	JSD↓
PC-GAN [1]	3.819	42.17	77.59	6.188	13.436	46.23	69.67	6.649
GCN-GAN [45]	4.713	39.04	89.13	6.669	15.354	39.84	77.86	21.71
Tree-GAN [38]	4.323	39.37	83.86	15.646	14.936	38.02	74.92	13.28
PointFlow [47]	3.688	44.98	66.39	1.536	13.631	41.86	66.13	12.47
ShapeGF [7]	3.306	50.41	61.94	1.059	13.175	48.53	56.17	5.996
DPM[26]	3.276	48.71	64.83	1.067	12.276	48.94	60.11	7.797
Ours	3.350	50.41	67.21	0.986	6.644	49.50	56.87	5.913

Table 1: Result of point cloud generation experiment. We adopt the base line from Luo and Hu [26]. Bolded value indicates the best performance method.

4 Experiments

We applied FHDM to distributions on various domains such as point cloud (general continuous distribution), distribution of climate and geography events on earth (continuous distribution on the sphere), unweighted graphs (distribution of binary matrices), and segmentation map of 2D image (high dimension categorical distribution). We demonstrate that

- 1. As a generalization of the fixed-time processes such as DDPM, the fixed-time scheme of FHDM is a generative model of higher quality for general continuous distribution (section 4.1).
- 2. As a versatile model, FHDM is able to learn the distribution in many different domains and it outperforms existing specifically designed generative models (see section 4.1).
- 3. The hitting time of FHDM is well-bounded and in several tasks, FHDM even requires much fewer diffusion steps than existing methods while generating higher quality samples (see section 4.2).

Besides, we also conduct experiments to understand the intuition of the first time hitting mechanism (section 4.2) and demonstrate the acceleration of the fast sampling approach introduced in Section 2.3.2 (see in Appendix A.6). We include the visualization of the generated samples in Appendix A.7. Please find the code at https://github.com/lushleaf/first_hitting_diffusion.

4.1 Generation Experiment

Point Cloud Generation Following Luo and Hu [26], we employ the ShapeNet dataset [8] to evaluate the generated point cloud. We compare our approach against several the state-of-the-art generative models including PC-GAN [1], GCN-GAN [45], Tree-GAN [38], PointFlow [47], ShapeGF [7] and DPM [26]. See Appendix A.5 for training details. Following Cai et al. [7], Luo and Hu [26], we use minimum matching distance (MMD) and the coverage score (COV) paired with Chamfer distance as well as 1-NN classifier accuracy and the Jensen-Shannon divergence (JSD) to evaluate the quality of the generated point cloud. We refer readers to Appendix A.5 for more details on the metrics. Same to Cai et al. [7], Luo and Hu [26], we evaluate the quality on two categories, Airplane and Chair and the generated and reference point clouds are normalized into a bounding box of $[-1, 1]^3$ at evaluation. Table 1 summarizes the results showing that FHDM achieves the best performance on most criterion.

Generating Distribution on Sphere We apply FHDM to generate distribution of occurrences of earth and climate science events on the surface of earth (which is approximated as a perfect sphere). Following De Bortoli et al. [12], we consider 4 datasets: volcanic eruption [29], earthquakes [28], floods [5] and wild fires [15]. We compared FHDM against the current the state-of-the-art baselines including Riemannian Continuous Normalizing Flows [27], Moser Flows [36], mixture of Kent distributions [33] and standard Score-Based Generative model on 2D plane followed by the inverse stereographic projection (Stereographic Score-Based) [16] and Riemannian Generative Model [12]. Same to De Bortoli et al. [12], we evaluate the method via the negative log-likelihood on the test set. We run our method for 5 independent trials and report the averaged metric with its standard deviation. We directly adopt the baseline result from De Bortoli et al. [12]. Table 2 summarizes the result. See Appendix A.5 for additional details.

	Volcano	Earthquake	Flood	Fire
Mixture of Kent [33]	-0.80 ± 0.47	0.33 ± 0.05	0.73 ± 0.07	-1.18 ± 0.06
Riemannian CNF [27]	-0.97 ± 0.15	0.19 ± 0.04	0.90 ± 0.03	-0.66 ± 0.05
Moser Flow [36]	-2.02 ± 0.42	-0.09 ± 0.02	0.62 ± 0.04	-1.03 ± 0.03
Stereographic Score-based [16]	-4.18 ± 0.30	-0.04 ± 0.11	1.31 ± 0.16	0.28 ± 0.20
Riemannian Score-based [12]	-5.56 ± 0.26	-0.21 ± 0.03	0.52 ± 0.02	-1.24 ± 0.07
Ours	-1.25 ± 0.18	-0.27 ± 0.02	0.29 ± 0.03	-1.24 ± 0.08

Table 2: Result on generating distribution of occurrences of earth and climate science events on the surface of earth. Bolded value indicates the best method.

Method	Community-small				Ego-small				Avg.
	Deg.	Clus.	Orbit.	Avg.	Deg.	Clus.	Orbit.	Avg.	
GraphVAE [39]	0.350	0.980	0.540	0.623	0.130	0.170	0.050	0.117	0.370
DeepGMG [23]	0.220	0.950	0.400	0.523	0.040	0.100	0.020	0.053	0.288
GraphRNN [48]	0.080	0.120	0.040	0.080	0.090	0.220	0.003	0.104	0.092
GNF [25]	0.200	0.200	0.110	0.170	0.030	0.100	0.001	0.044	0.107
EDP-GNN[30]	0.053	0.144	0.026	0.074	0.052	0.093	0.007	0.050	0.062
Ours	0.009	0.105	0.009	0.041	0.019	0.040	0.005	0.021	0.031

Table 3: Result on graph generation experiment. We report the averaged performance of our approach based on 5 independent runs, giving 0.0013 standard deviation of the averaged metric. The results of the other baselines are directly adopted from Niu et al. [30]. Bolded value indicates the best method.

Graph Generation We apply FHDM to generate (unweighted) graph that can be represented using binary adjacency matrix. Following the experiment setup in You et al. [48], Liu et al. [25], Niu et al. [30], we compare methods on two widely used benchmark datasets, Community-small and Ego-small. We apply the EDP-GNN [30] that preserves the node permutation invariance to approximate the drift. We compare FHDM against GraphRNN [48], GNF [25], GraphVAE [39] and DeepGMG [23]. The maximum mean discrepancy (MMD) over three graph statistics (1. degree distribution; 2. cluster coefficient distribution; 3. the number of orbits with 4 nodes) proposed by You et al. [48] is used to evaluate the quality of the generative graphs. For our approach, we run 5 independent trails and report the averaged performance. See Appendix A.5 for additional training details. Table 3 summarizes the result, suggesting considerable improvement over the baselines.

Segmentation Map Generation FHDM can also be applied to generate high dimensional categorical distribution such as the segmentation map of a 2D image. Following Hooeboom et al. [19], we aim to learn a model to generate the segmentation map of cityscapes dataset, in which the value of each pixel represents the category of the object that pixel belongs to. Following the setup in Hooeboom et al. [19], there are in total 8 categories and the value at each pixel is coded using one-hot vector. We compare our approach with uniform dequantization [44], variational dequantization [17], three variants of argmax flow [19] and multinomial diffusion [19]. Following Hooeboom et al. [19], we evaluate the quality of generative model by evidence lower bound (ELBO) and importance weighted bound (IWBO) [6] (when it is available) with 1000 samples measured in bits per pixel. For our method, we run 5 independent trials and report the averaged metric and its standard deviation. The other baselines are directly adopted from Hooeboom et al. [19]. The result is summarized in Table 4. See Appendix A.5 for additional details.

Method	ELBO	IWBO
Round / Unif [44]	1.010	0.930
Round / Var [17]	0.334	0.315
Argmax / Softplus thres. [19]	0.303	0.290
Argmax / Gumbel dist. [19]	0.365	0.341
Argmax / Gumbel thres. [19]	0.307	0.287
Multinomial Diffusion [19]	0.305	-
Ours	0.066	0.065

Table 4: Result for segmentation map generation. We run our method for 5 independent runs and report the averaged performance. FHDM gives 0.003/0.006 standard deviation of ELBO/IWBO.

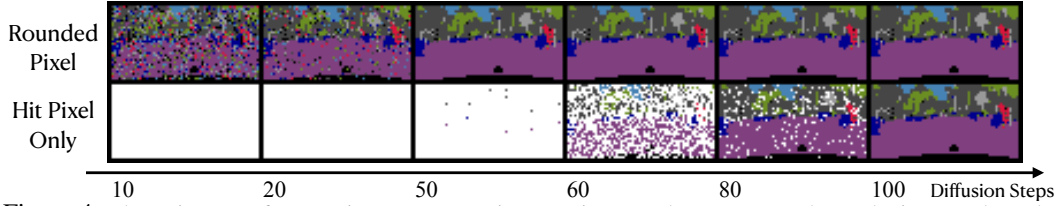


Figure 4: The trajectory of generating a segmentation map image. The upper row shows the image where the category of all pixels are decided based on the argmax (i.e., rounding) of all the 8 scores. The lower row only plots the hit pixels of the snapshots.

4.2 Analysis

Hitting time distribution We study the hitting time distribution given by the optimized network, which is summarized in Figure 5. Our first hitting diffusion model is able to hit the domain in a well-bounded time. It is worth remarking that for Boolean and categorical distribution, *FHDM generates higher quality samples with much fewer diffusion steps*. For example, in graph generation, FHDM on average takes about 100 steps while the previous approach such as Niu et al. [30] requires 6K steps. Similarly, in segmentation map generation, FHDM takes about 90 steps on average while the multinomial diffusion [19] needs 4K steps. Decreasing the number of diffusion steps in those approaches will degenerate the performance. For example, if we only use 120 diffusion steps in Niu et al. [30] the averaged performance becomes 0.306 which is much worse. See Appendix A.6 for detailed result.

Why we can stop at hitting time The key feature of FHDM that is we stop the diffusion when it hits the domain rather than keep it running for a pre-fixed time. We explore more the intuition behind such a process. In figure 4 we visualize the trajectory of generating a segmentation map. By looking at the image snapshot in the upper row where the value of each pixel is decided by the argmax (i.e. rounding) of the 8 scores, we observe that the global contour of the image is already determined at a very early time (i.e., step 20) while the refinement of local details is almost finished at step 50. Our first hitting model exploits such property to stop the diffusion of the hit pixels that the model has enough confidence about its value making the generating process of the rest pixels easier.

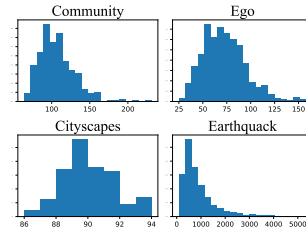


Figure 5: Hitting time distributions for different data distributions.

5 Conclusion

We propose the first hitting diffusion model (FHDM), which generalizes the fixed-time diffusion process and allows instance-dependent adaptive diffusion steps. Leveraging the idea of exit distribution, FHDM provides a unified framework for learning distribution in various special domains. Despite the good functionality, FHDM takes slightly larger training overhead, which is partially solved by the our fast sampling tricks.

References

- [1] Panos Achlioptas, Olga Diamanti, Ioannis Mitliagkas, and Leonidas Guibas. Learning representations and generative models for 3d point clouds. In *International conference on machine learning*, pages 40–49. PMLR, 2018.
- [2] Brian DO Anderson. Reverse-time diffusion equation models. *Stochastic Processes and their Applications*, 12(3):313–326, 1982.
- [3] Andrei N Borodin and Paavo Salminen. *Handbook of Brownian motion-facts and formulae*. Springer Science & Business Media, 2015.
- [4] Bruno Bouchard, Stefan Geiss, and Emmanuel Gobet. First time to exit of a continuous itô process: General moment estimates and l_1 -convergence rate for discrete time approximations. *Bernoulli*, 23(3):1631–1662, 2017.
- [5] G. Brakenridge. Global active archive of large flood events. 2017. URL <http://floodobservatory.colorado.edu/Archives/index.html>.
- [6] Yuri Burda, Roger Grosse, and Ruslan Salakhutdinov. Importance weighted autoencoders. *arXiv preprint arXiv:1509.00519*, 2015.
- [7] Ruojin Cai, Guandao Yang, Hadar Averbuch-Elor, Zekun Hao, Serge Belongie, Noah Snavely, and Bharath Hariharan. Learning gradient fields for shape generation. In *European Conference on Computer Vision*, pages 364–381. Springer, 2020.
- [8] Angel X Chang, Thomas Funkhouser, Leonidas Guibas, Pat Hanrahan, Qixing Huang, Zimo Li, Silvio Savarese, Manolis Savva, Shuran Song, Hao Su, et al. Shapenet: An information-rich 3d model repository. *arXiv preprint arXiv:1512.03012*, 2015.
- [9] Nanxin Chen, Yu Zhang, Heiga Zen, Ron J Weiss, Mohammad Norouzi, and William Chan. Wavegrad: Estimating gradients for waveform generation. *arXiv preprint arXiv:2009.00713*, 2020.
- [10] Tianrong Chen, Guan-Hong Liu, and Evangelos A Theodorou. Likelihood training of schrödinger bridge using forward-backward sdes theory. *arXiv preprint arXiv:2110.11291*, 2021.
- [11] Valentin De Bortoli, James Thornton, Jeremy Heng, and Arnaud Doucet. Diffusion schrödinger bridge with applications to score-based generative modeling. *Advances in Neural Information Processing Systems*, 34, 2021.
- [12] Valentin De Bortoli, Emile Mathieu, Michael Hutchinson, James Thornton, Yee Whye Teh, and Arnaud Doucet. Riemannian score-based generative modeling. *arXiv preprint arXiv:2202.02763*, 2022.
- [13] Prafulla Dhariwal and Alexander Nichol. Diffusion models beat gans on image synthesis. *Advances in Neural Information Processing Systems*, 34, 2021.
- [14] Joseph L Doob and JI Doob. *Classical potential theory and its probabilistic counterpart*, volume 549. Springer, 1984.
- [15] EOSDIS. Land, atmosphere near real-time capability for eos (lance) system operated by nasa’s earth science data and information system (esdis). 2020. URL <https://earthdata.nasa.gov/earth-observation-data/near-real-time/firms/active-fire-data>.
- [16] Mevlana C Gemici, Danilo Rezende, and Shakir Mohamed. Normalizing flows on riemannian manifolds. *arXiv preprint arXiv:1611.02304*, 2016.
- [17] Jonathan Ho, Xi Chen, Aravind Srinivas, Yan Duan, and Pieter Abbeel. Flow++: Improving flow-based generative models with variational dequantization and architecture design. In *International Conference on Machine Learning*, pages 2722–2730. PMLR, 2019.
- [18] Jonathan Ho, Ajay Jain, and Pieter Abbeel. Denoising diffusion probabilistic models. *Advances in Neural Information Processing Systems*, 33:6840–6851, 2020.

- [19] Emiel Hoogeboom, Didrik Nielsen, Priyank Jaini, Patrick Forré, and Max Welling. Argmax flows and multinomial diffusion: Learning categorical distributions. *Advances in Neural Information Processing Systems*, 34, 2021.
- [20] Jian Huang, Yuling Jiao, Lican Kang, Xu Liao, Jin Liu, and Yanyan Liu. Schrödinger-föllmer sampler: Sampling without ergodicity. *arXiv preprint arXiv:2106.10880*, 2021.
- [21] Diederik P Kingma and Jimmy Ba. Adam: A method for stochastic optimization. *arXiv preprint arXiv:1412.6980*, 2014.
- [22] Zhifeng Kong, Wei Ping, Jiaji Huang, Kexin Zhao, and Bryan Catanzaro. Diffwave: A versatile diffusion model for audio synthesis. In *International Conference on Learning Representations*, 2020.
- [23] Yujia Li, Oriol Vinyals, Chris Dyer, Razvan Pascanu, and Peter Battaglia. Learning deep generative models of graphs. *arXiv preprint arXiv:1803.03324*, 2018.
- [24] Robert Shevilevich Liptser and Al’bert Nikolaevich Shiriaev. *Statistics of random processes: General theory*, volume 394. Springer, 1977.
- [25] Jenny Liu, Aviral Kumar, Jimmy Ba, Jamie Kiros, and Kevin Swersky. Graph normalizing flows. *Advances in Neural Information Processing Systems*, 32, 2019.
- [26] Shitong Luo and Wei Hu. Diffusion probabilistic models for 3d point cloud generation. In *Proceedings of the IEEE/CVF Conference on Computer Vision and Pattern Recognition*, pages 2837–2845, 2021.
- [27] Emile Mathieu and Maximilian Nickel. Riemannian continuous normalizing flows. *Advances in Neural Information Processing Systems*, 33:2503–2515, 2020.
- [28] NGDC/WDS. Ncei/wds global significant earthquake database. . URL <https://www.nci.noaa.gov/access/metadata/landing-page/bin/iso?id=gov.noaa.ngdc.mgg.hazards:G012153>.
- [29] NGDC/WDS. Ncei/wds global significant volcanic eruptions database. . URL <https://www.nci.noaa.gov/access/metadata/landing-page/bin/iso?id=gov.noaa.ngdc.mgg.hazards:G10147>.
- [30] Chenhao Niu, Yang Song, Jiaming Song, Shengjia Zhao, Aditya Grover, and Stefano Ermon. Permutation invariant graph generation via score-based generative modeling. In *International Conference on Artificial Intelligence and Statistics*, pages 4474–4484. PMLR, 2020.
- [31] Bernt Oksendal. *Stochastic differential equations: an introduction with applications*. Springer Science & Business Media, 2013.
- [32] Michele Pavon, Giulio Trigila, and Esteban G Tabak. The data-driven schrödinger bridge. *Communications on Pure and Applied Mathematics*, 74(7):1545–1573, 2021.
- [33] David Peel, William J Whiten, and Geoffrey J McLachlan. Fitting mixtures of kent distributions to aid in joint set identification. *Journal of the American Statistical Association*, 96(453):56–63, 2001.
- [34] Stefano Peluchetti. Non-denoising forward-time diffusions. 2021.
- [35] Olaf Ronneberger, Philipp Fischer, and Thomas Brox. U-net: Convolutional networks for biomedical image segmentation. In *International Conference on Medical image computing and computer-assisted intervention*, pages 234–241. Springer, 2015.
- [36] Noam Rozen, Aditya Grover, Maximilian Nickel, and Yaron Lipman. Moser flow: Divergence-based generative modeling on manifolds. *Advances in Neural Information Processing Systems*, 34, 2021.
- [37] Simo Särkkä and Arno Solin. *Applied stochastic differential equations*, volume 10. Cambridge University Press, 2019.

- [38] Dong Wook Shu, Sung Woo Park, and Junseok Kwon. 3d point cloud generative adversarial network based on tree structured graph convolutions. In *Proceedings of the IEEE/CVF International Conference on Computer Vision*, pages 3859–3868, 2019.
- [39] Martin Simonovsky and Nikos Komodakis. Graphvae: Towards generation of small graphs using variational autoencoders. In *International conference on artificial neural networks*, pages 412–422. Springer, 2018.
- [40] Jascha Sohl-Dickstein, Eric Weiss, Niru Maheswaranathan, and Surya Ganguli. Deep unsupervised learning using nonequilibrium thermodynamics. In *International Conference on Machine Learning*, pages 2256–2265. PMLR, 2015.
- [41] Yang Song and Stefano Ermon. Generative modeling by estimating gradients of the data distribution. *Advances in Neural Information Processing Systems*, 32, 2019.
- [42] Yang Song and Stefano Ermon. Improved techniques for training score-based generative models. *Advances in neural information processing systems*, 33:12438–12448, 2020.
- [43] Yang Song, Jascha Sohl-Dickstein, Diederik P Kingma, Abhishek Kumar, Stefano Ermon, and Ben Poole. Score-based generative modeling through stochastic differential equations. In *International Conference on Learning Representations*, 2020.
- [44] Benigno Uria, Iain Murray, and Hugo Larochelle. Rnade: The real-valued neural autoregressive density-estimator. *Advances in Neural Information Processing Systems*, 26, 2013.
- [45] Diego Valsesia, Giulia Fracastoro, and Enrico Magli. Learning localized generative models for 3d point clouds via graph convolution. In *International conference on learning representations*, 2018.
- [46] Gefei Wang, Yuling Jiao, Qian Xu, Yang Wang, and Can Yang. Deep generative learning via schrödinger bridge. In *International Conference on Machine Learning*, pages 10794–10804. PMLR, 2021.
- [47] Guandao Yang, Xun Huang, Zekun Hao, Ming-Yu Liu, Serge Belongie, and Bharath Hariharan. Pointflow: 3d point cloud generation with continuous normalizing flows. In *Proceedings of the IEEE/CVF International Conference on Computer Vision*, pages 4541–4550, 2019.
- [48] Jiaxuan You, Rex Ying, Xiang Ren, William Hamilton, and Jure Leskovec. Graphrnn: Generating realistic graphs with deep auto-regressive models. In *International conference on machine learning*, pages 5708–5717. PMLR, 2018.
- [49] Linqi Zhou, Yilun Du, and Jiajun Wu. 3d shape generation and completion through point-voxel diffusion. In *Proceedings of the IEEE/CVF International Conference on Computer Vision*, pages 5826–5835, 2021.

A Appendix

A.1 Algorithm for Learning Categorical Data

The over all training algorithm for learning categorical generative models is similar to the other cases. To simulate the conditioned process, given any exit point $x \in C_{d,m} \subseteq B_d$, we know that $\mathbb{Q}^{C_{d,m}}(\cdot | Z_\tau = x) = \mathbb{Q}^{B_d}(\cdot | Z_\tau = x)$ and thus (5) can be reused. The training of the network is also similar, the only difference is that we have the additional term $\nabla_z \log \text{Ber}(\Omega | Z_t)$ in the output of the network to ensure that the generative process in proposition 2.10 is guaranteed to hit Ω when it exists V . The training loss is thus

$$\mathcal{L}(\theta) = \frac{1}{2} \mathbb{E}_{\substack{x \sim \Pi^* \\ Z \sim \mathbb{Q}^x}} \left[\int_0^\tau \left\| \mathbb{I}\{Z_t \in C_{d,m}\} \circ (f_t^\theta(Z_t) + \nabla_{Z_t} \log \text{Ber}(\Omega | Z) - \nabla_{Z_t} \log \text{Ber}(Z_t | x)) \right\|^2 dt - \log p_0^\theta(Z_0) \right] + \text{const.}$$

A.2 Practical Algorithm

We give a detailed practical algorithm.

Discretized process Suppose that the diffusion step size at step k is ϵ_k . Given the exit point x , the discretized conditioned process can be simulated by

$$Z_{t_{k+1}} = \left(b_{t_k}(Z_{t_k}) + \sigma_{t_k}^2(Z_{t_k}) \nabla_z \log h_{t_k}^{\Pi^*}(Z_{t_k}) \right) \epsilon_k + \sqrt{\epsilon_k} \sigma_{t_k}(Z_{t_k}) \xi_k, \quad Z_{t_0} \sim \mathbb{Q}_0^{\Pi^*}, \quad (16)$$

where $\xi_k \sim \mathcal{N}(0, I)$ is a standard Gaussian noise. Note that (16) is terminated at t_k when Z_{t_k} firstly hits the desired domain. Alternatively, we can first sample (discretized) unconditioned process by

$$Z_{t_{k+1}} = b_{t_k}(Z_{t_k}) \epsilon_k + \sqrt{\epsilon_k} \sigma_{t_k}(Z_{t_k}) \xi_k, \quad Z_{t_0} \sim \mathbb{Q}_0^{\Pi^*}, \quad (17)$$

And then apply the rotation operators defined in Section 2.3.2 such that the sampled trajectory ends at x .

A simplified loss Similar to Song and Ermon [41], Ho et al. [18], we use a stochastic version of loss (15), in which we only uniformly sample temporal snapshots to compute the loss.

$$\hat{\mathcal{L}}(\theta) = \frac{1}{2} \mathbb{E}_{\mathbb{Q}^{\Pi^*}} \mathbb{E}_{t \sim \text{Unif}\{0, \dots, \tau\}} \left[\left\| \sigma_t(Z_t)^{-1} (s_t^\theta(Z_t) - b_t(Z_t | Z_\tau)) \right\|^2 - \log p_0^\theta(Z_0) \right] + \text{const.} \quad (18)$$

In Algorithm A.2, we summarize the training procedure of FHDM.

Algorithm 2 Learning Generative Models by First Hitting Diffusion

Inputs: A data $\{x^{(i)}\}$ drawn from Π^* on Ω . A baseline process \mathbb{Q} and a model \mathbb{P}^θ that are absorbing to Ω .

Goal: Find θ such that $\mathbb{P}_\Omega^\theta \approx \Pi^*$.

Training: By minimizing $\mathcal{L}(\theta)$.

(Optional) Pre-simulate unconditioned trajectories of \mathbb{Q} using (17).

for training iters **do**

 Get a mini batch of data from training set.

 //Optionally, we can use fast bridge sampling tricks to get conditioned sample by rotating // pre-simulated unconditioned trajectories.

 Sample trajectories $\mathbb{Q}(\cdot | Z_\tau = x)$ for each data x in the mini batch using (16)

 Calculate the mini-batch loss $\mathcal{L}(\theta)$ defined in Equ (18).

 Apply gradient descent to update θ .

end for

A.3 Sampling with first hitting h -transform

The h -transform formula on first hitting diffusion readily provides a simple mechanism for approximate sampling from Π^* : Assume the baseline process X is designed simple enough such that the

conditional harmonic measure $\mathbb{Q}_\Omega(\cdot | Z_t = z)$ is easy to calculate, then we can approximately $h_t^{\Pi^*}(z)$ in (10) by Monte Carlo sampling from $\mathbb{Q}_\Omega(\cdot | Z_t = z)$:

$$h_t^{\Pi^*}(z) \approx \frac{1}{m} \sum_{i=1}^m \pi^*(x^{(i)}), \quad x^{(i)} \sim \mathbb{Q}_\Omega(\cdot | Z_t = z),$$

use it simulate process (9). The gradient $\nabla \log h_t^{\Pi^*}$ can be approximated with either the reparameterization method or score function method. See Algorithm A.3.

Algorithm 3 Approximate Sampling by First Hitting Diffusion

Goal: Draw sample from Π^* on $\Omega \in \mathbb{R}^d$.

Prepare a baseline diffusion process $Z \sim \text{It}_{0,\Omega}(b, \sigma)$ in (3) with exit distribution $\mathbb{Q}_\Omega(A | Z_t = z) = \mathbb{Q}(Z_\tau \in A | Z_t = z)$. Let $h = d\Pi^*/d\mathbb{Q}_\Omega(\cdot | Z_0 = z_0)$ be the density ratio between Π^* and $\mathbb{Q}_\Omega(\cdot | Z_0 = z_0)$, where the initialization $Z_0 = z_0$ is in $V \setminus \Omega$.

Simulate the following process $\{\hat{Z}_t\}$ starting from $\hat{Z}_0 = z_0$ and stop at the first hitting time $\tau = \inf\{t \geq 0: \hat{Z}_t \in \Omega\}$:

$$d\hat{Z}_t = \left(b_t(\hat{Z}_t) + \sigma_t^2(\hat{Z}_t) \nabla_z \log \hat{h}_t(\hat{Z}_t) \right) dt + \sigma_t(\hat{Z}_t) dW_t, \quad (19)$$

where $\hat{h}_t(z) = \frac{1}{m} \sum_{i=1}^m \pi^*(x^{(i)})$, where $\{x^{(i)}\}_{i=1}^m$ is drawn i.i.d. from $\mathbb{Q}_\Omega(\cdot | Z_t = z)$; the derivative $\nabla_z \log \hat{h}_t(z)$ can be calculated by either the reparameterization trick or score function method.

Return \hat{Z}_τ as an approximate draw from Π^* .

A.4 Connection with SMLD and DDPM

Standard diffusion generative models such as SMLD and DDPM determinates the diffusion process at a fixed time, which can be included as a special first hitting model as shown in Example 2.4. We clarify the connection to SMLD and DDPM for completeness here. In this case, we set \mathbb{Q} to be an Ornstein-Uhlenbeck (O-U) process $dZ_t = \alpha_t Z_t dt + \sigma_t dW_t$ initialized at $Z_0 \sim \mathcal{N}(\mu_0, v_0)$ and stopped at a deterministic time $t = t$, where $\alpha_t \in \mathbb{R}$ and $\sigma_t \geq 0, v_0 \geq 0, \forall t$. This is a Gaussian process. Let $Z_t \sim \mathcal{N}(\mu_t, v_t)$. Denote by $\bar{Z}_t = Z_{t-t}$ the time reversed process, which follows [2]

$$d\bar{Z}_t = \left(-\alpha_{t-t} \bar{Z}_t + \sigma_{t-t}^2 \frac{\mu_{t-t} - \bar{Z}_t}{v_{t-t}} \right) dt + \sigma_{t-t} d\bar{W}_t,$$

where \bar{W}_t is a copy of standard Brownian motion. If we set $v_0 \rightarrow +\infty$ in the initial Z_0 , we expect to have $v_t \rightarrow +\infty$ under proper regularity conditions on α_t and σ_t , the second term in the drift of \bar{Z}_t is canceled, yielding $d\bar{Z}_t = -\alpha_{t-t} \bar{Z}_t dt + \sigma_{t-t} d\bar{W}_t$. This then reduces to the processes used in SMLD ($\alpha_t = 0$), and DDPM and SDE method in [43] ($\alpha_t > 0$). This framework of learning fixed-time diffusion models using bridge processes are explored separately in a recent work [34]. The authors devote more in-depth discussions on the fixed-time diffusion case in a separate work.

A.5 Additional Experiment Details

A.5.1 Point Cloud Generation

Training details The ShapeNet dataset contains 51,127 shapes from 55 categories and is randomly split training, testing and validation set by the ratio 80%, 15% and 5%. For each shape, we sample 2048 points to acquire the point clouds and normalize each of them to zero mean and unit variance.

We build our method on Luo and Hu [26] in which the encoder of a flow-based model is used to learn a latent code of the shape and conditioning on the shape latent code, the point are independently generated based on a diffusion model. We substitute the DDPM-type [18] of diffusion model with ours and all the other components remain the same. Each point is generated using 100 diffusion steps and the step size linearly decays starting from 0.02 to 10^{-4} . We use the same network architecture for flow-based model and point diffusion network. We train the model for 1M steps with batch size 128 using Adam optimizer [21].

More Details on Evaluation Metrics Both MMD, JSD and 1-NN measures the fidelity of the generated samples. The 1-NN score is the accuracy of 1-NN classifier in predicting whether a point cloud is generated by the model or from the data. Lower 1-NN scores suggest higher quality. MMD and JSD measures the probability distance between the point distributions of the generated set and the reference set from data and thus lower MMD and JSD means higher quality. COV detects mode-collapse and higher COV suggests more diverse generated samples.

A.5.2 Generating Distribution on Sphere

Training details All datasets are split into training, validation and test sets with (0.8, 0.1, 0.1) proportions. We train the model for 2000 iterations using Adam Optimizer [21] with learning rate 0.05 and batch size 128. We use a three-layer MLP with 100 hidden units and ReLU activation to approximate the drift. We set the maximum diffusion step as 10K with step size 5×10^{-4} . The model on average takes 1K steps to hit and seldom takes more than 5K to hit. See section 4.2 for more details on the hitting time distribution.

A.5.3 Graph Generation

Training details We set the maximum number of SDE steps as 10K, and it takes on average about 100 steps to hit. See section 4.2 for more detailed analysis. At each step, we set the standard deviation of gaussian noise as 0.5. We initialize all the coordinate 0.5 and stop the updating of a coordinate at the first time its distance to 0 or 1 is less than 0.05. We use the same network architecture and training pipeline as Niu et al. [30]. Adam optimizer [21] with 0.001 learning rate is applied. Batch size is set to 32 and for each graph, we randomly sample 6 snapshot in the trajectory for training. The score matching loss of a hit coordinate is masked out at training.

A.5.4 Segmentation Map Generation

Training details Our network architecture and training pipeline is almost the same as the multinomial diffusion model proposed in Hoogetboom et al. [19]. The only architecture difference is that Hoogetboom et al. [19] first feed the image into an embedding layer before passing to the subquential U-Net [35] like structure while we use a linear layer with the same output dimension. This is because the multinomial diffusion model [19] is a discrete diffusion in which the value at each pixel is considered to be discrete while FHDM is a continuous diffusion. We set the number of maximum diffusion steps to be 100 and the step size to be 0.1. We apply step-decayed Gaussian noise at different diffusion steps, in which the standard deviation at initial is 1 and decay to half at step 500 and 750. The pixel is hit and stopped to update at the first time its largest categorical score (among 8 of them) is greater than $1 - \epsilon$ with $\epsilon = 0.01$. We apply the same data augmentation and train the model for 500 epochs with batch size 64, learning rate 10^{-4} and Adam optimizer [21]. For each image in the batch, we randomly sample one time snapshot along the diffusion trajectory for training.

For this task, we apply the fast bridge sampling method proposed in Section 2.3.2. At the beginning of each epoch, we generate $10 \times \text{batch size} \times H \times W$ unconditional SDE trajectories where H, W is the height and width of the images. At the training time, to simulate the SDE trajectories of a given image in the training set, for each pixel, we randomly select one saved unconditional SDE trajectories and rotates it such that it ends at that pixel.

A.6 Additional Experiment Results

Number of diffusion steps When we restrict the number of diffusion steps of EDP-GNN [30], the second-best approach, similar to that of FHDM (120), we observe a significant performance drop. As shown in Table 5, the performance of EDP-GNN degenerates badly when we decrease its diffusion steps from 4K to 120.

Acceleration by fast sampling We give brief analysis on the acceleration effect of the fast bridge sampling method described in Section 2.3.2. When applied to the segmentation generation experiment, we pre-simulate 640 trajectories in the beginning of each training epoch which gives 2.5x acceleration from 24.3 cpu time/epoch to 9.8 cpu time/epoch, making the training time of FHDM is comparable to Hoogetboom et al. [19] (6.5 cpu time/epoch). We remark that although FHDM has slightly larger training overhead, its only requires less than 100 diffusion steps at inference, giving a 40x speed up compared with Hoogetboom et al. [19].

Method	Community-small				Ego-small				Avg
	Deg.	Clus.	Orbit.	Avg.	Deg.	Clus.	Orbit.	Avg.	
EDP-GNN	0.053	0.144	0.026	0.074	0.052	0.093	0.007	0.050	0.062
EDP-GNN (step=120)	0.586	0.253	0.705	0.515	0.141	0.114	0.036	0.097	0.306
Ours	0.004	0.104	0.001	0.036	0.019	0.047	0.005	0.024	0.030

Table 5: Comparing FHDM with EDP-GNN with similar diffusion steps.

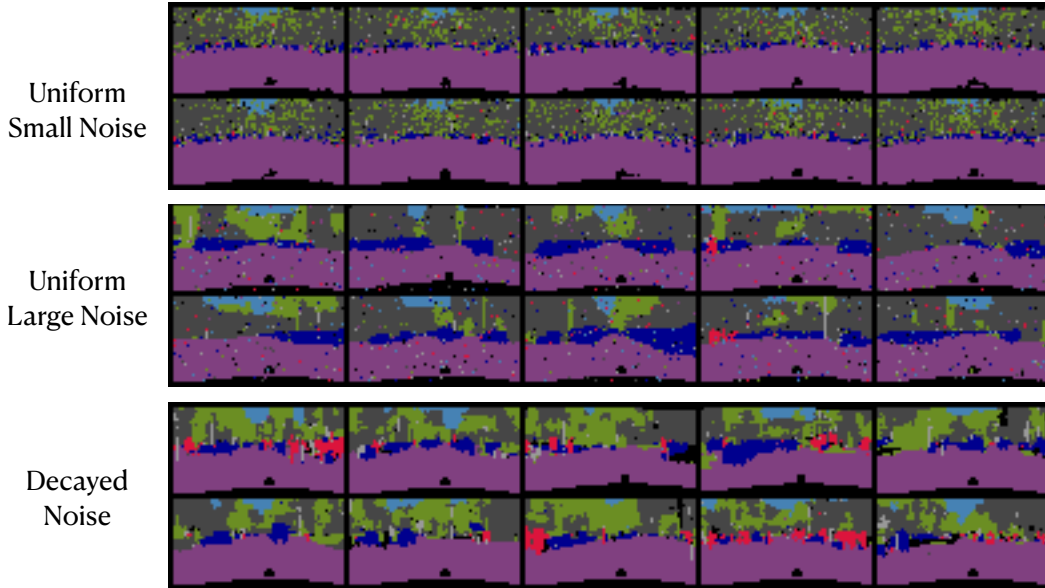


Figure 6: Compare the generated segmentation maps with different noise schedule.

Ablation studies on noise schedule In practice, we observe that the design of the noise schedule can be important for some tasks such as segmentation generation. We show samples generated by FHDM with uniformly small noise (std=0.25), uniformly large noise (std=1) and decayed noise as described in Section in 4.1. It is worth noticing that using a uniformly small noise generates over-smoothed and degenerated images that fail to reveal the details while using a uniformly large noise gives more diverse but noisy images. In comparison, the decaying noise generates high-quality diverse images with fine details.

A.7 Visualization of Generated Samples

Point Cloud Generation Please see Figure 7 and 8 for the generated airplane and chair point cloud using FHDM.

Generating Distribution on Sphere Please see Figure 11 for the generated graphs using FHDM.

Segmentation Map Generation Please see Figure 9 for the generated distributions on sphere by FHDM.

Graph Generation Please see Figure 11 for the generated graphs using FHDM.

Segmentation Map Generation Please see Figure 10 for the generated segmentation maps by FHDM.

A.8 Discretization Error Analysis

Consider the following Ito process

$$dZ_t = b(Z_t)dt + \sigma(Z_t)dW_t$$

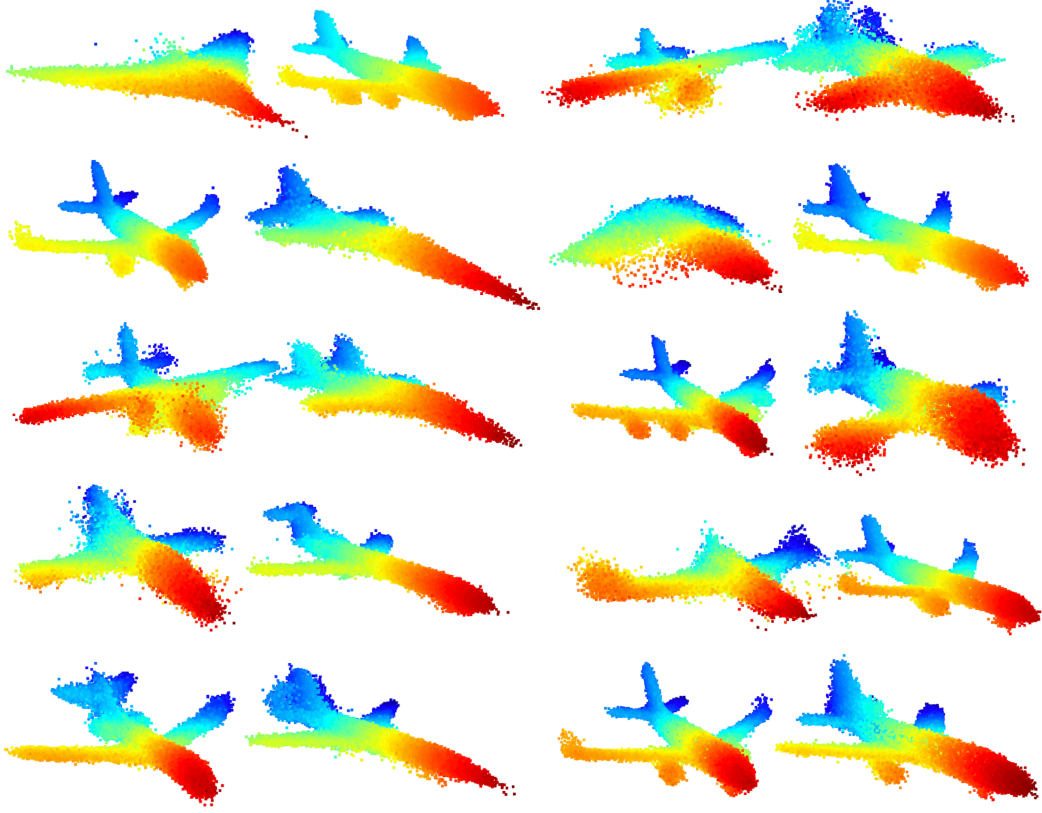


Figure 7: The generated airplane point cloud by FHDM.

and a open subset $V \subseteq \mathbb{R}^d$. Here $b \in \mathbb{R}^d$ is the drift and $\sigma \in \mathbb{R}^{d \times d}$ is the diffusion matrix. We stop the process when Z_t hit the domain Ω and denote the hitting time as $\tau := \inf_{t \geq 0} \{Z_t \notin V\}$. We consider the discretalization error of the conditional distribution π_T with temporal truncation T , i.e.,

$$\pi_T := \text{law of } X_\tau \mid \tau \leq T.$$

This corresponds to the situation that we discard the non-hit process after waiting for T time. To simulate the above process, we consider the Euler discretization on $[0, T]$. Suppose R is a set of grid points on $[0, T]$ in which we define

$$r_t = \max\{r \in R : r \leq t\}.$$

The Euler discretized process is thus defined as

$$d\bar{Z}_t = b(\bar{Z}_{r_t}) + \sigma(\bar{Z}_{r_t})dW_t.$$

And similarly, we can define its (discretize) stopping time $\bar{\tau} := \min_{r \in R} \{r : \bar{Z}_{r_t} \notin V\}$. We want to bound the discrepancy between π_T and the following distribution

$$\bar{\pi}_T := \text{law of } \bar{X}_{\bar{\tau}} \mid \bar{\tau} \leq T.$$

We consider the Wassestein distance $\mathcal{W}[\bar{\pi}_T, \pi_T]$ for measuring the discrepancy. In this section, $\|\cdot\|$ is vector norm when applied to vector and is matrix operator norm when applied to matrix.

Assumption 1. b and σ is L -Lipschitz and $\sup_z (\|b(z)\| + \|\sigma(z)\|) \leq L$.

Assumption 2. There exists a bounded C_b^2 function $\delta : \mathbb{R}^d \rightarrow \mathbb{R}$ such that $\delta > 0$ on V , $\delta = 0$ on Ω and $\delta < 0$ on $\mathbb{R}^d \setminus (V \cup \Omega)$ and satisfies the non-characteristic boundary condition $\|\sigma \nabla \delta\| \geq 2L^{-1}$ on $\{\|\delta\| \leq r\}$ for some $r > 0$.

Assumption 1 is a standard assumption on the Lipschitz continuity and boundedness on the drift and diffusion function. Assumption 2 is more on a technical condition and is introduced in Bouchard et al. [4] and intuitively it can be understood in the way that there exists a bounded smooth function that can indicate whether we are within V or out of V .

Theorem 1. Let $\Delta := \min_{r_t \neq r_{t'}} |r_t - r_{t'}|$. Under Assumption 1, 2 and assume that T is properly large such that $\mathbb{P}(\tau \geq T - 1) \leq 1/4$, we have, there exists $\epsilon > 0$ such that for any $\Delta \leq \epsilon$,

$$\mathcal{W}^2[\bar{\pi}_T, \pi_T] = O(\exp(cT)\Delta),$$

for some absolute constant $c < \infty$.

Intuitively, we show that when T is properly large (which is true in practice as we should wait the process a reasonably enough time for hitting) and the step size is small enough, the discretize error is small.

Proof. Throughout the proof, c denotes absolute constant and may vary in different lines. We consider the temporal augmented process $Y_t = [Z_t, t]$ in which

$$dY_t = \tilde{b}(Y_t)dt + \tilde{\sigma}(Y_t)dW_t.$$

Here \tilde{b} and $\tilde{\sigma}$ are defined as

$$\tilde{b}(y) = [b(x), 1], \tilde{\sigma}_y(y) = \begin{bmatrix} \sigma(y) & \mathbf{0} \\ \mathbf{0}^\top & 0 \end{bmatrix}.$$

It is not hard to verify the Lipschitz continuity and boundedness of \tilde{b} and $\tilde{\sigma}$. We also define the hitting set of the process Y_t by $\tilde{V} = \{y : x \in V \text{ or } t < T + 1\}$. It is easy to show that \tilde{V} is a closed subset of \mathbb{R}^{d+1} and the stopping time $\tau := \inf_{t \geq 0} \{t : Y_t \notin \tilde{V}\} \leq T + 1$. Similarly, we can define the discretized version

$$d\bar{Y}_t = \tilde{b}(\bar{Y}_{r_t})dt + \tilde{\sigma}(\bar{Y}_{r_t})dW_t.$$

Here we slightly abuse the notation of τ and $\bar{\tau}$, making them denoting the hitting time of process Y_t and \bar{Y}_t rather than Z_t and \bar{Z}_t . We introduce the following Lemma used in Bouchard et al. [4].

Lemma 1 (Theorem 3.11 in Bouchard et al. [4]). *Under assumption 1 and 2, there exists $\epsilon > 0$ such that when $\Delta \leq \epsilon$, $\mathbb{E}[|\tau - \bar{\tau}|] \leq c\Delta^{1/2}$ for some constant $c > 0$.*

Note that

$$\mathbb{E}[|\bar{Y}_{\bar{\tau}} - Y_\tau|^2 \mid \bar{\tau} \leq T] \leq \int \mathbb{E}[|\bar{Y}_{\bar{\tau}} - Y_\tau|^2 \mid |\bar{\tau} - \tau| = s, \bar{\tau} \leq T] \Pr(|\bar{\tau} - \tau| = s \mid \bar{\tau} \leq T) ds.$$

Note that we can decompose

$$\begin{aligned} & \mathbb{E}[|\bar{Y}_{\bar{\tau}} - Y_\tau|^2 \mid |\bar{\tau} - \tau| = s, \bar{\tau} \leq T] \\ & \leq 2\mathbb{E}[|\bar{Y}_{\bar{\tau}} - Y_{\bar{\tau}}|^2 \mid |\bar{\tau} - \tau| = s, \bar{\tau} \leq T] + 2\mathbb{E}[|Y_{\bar{\tau}} - Y_\tau|^2 \mid |\bar{\tau} - \tau| = s, \bar{\tau} \leq T]. \end{aligned}$$

Using Lemma A.2 in Bouchard et al. [4] and Holder's inequality, we have

$$\leq \mathbb{E}[|\bar{Y}_{\bar{\tau}} - Y_{\bar{\tau}}|^2 \mid |\bar{\tau} - \tau| = s, \bar{\tau} \leq T] \leq \sup_{t \in [0, T+s]} \|\bar{Y}_{\bar{\tau}} - Y_{\bar{\tau}}\|^2 \leq c\Delta,$$

for some constant c . Also, by the boundedness of \tilde{b}

$$\|Y_{\bar{\tau}} - Y_\tau\| = \left\| \int_{\min(\bar{\tau}, \tau)}^{\max(\bar{\tau}, \tau)} \tilde{b}(Y_t) dt \right\| \leq (L+1)|\tau - \bar{\tau}|.$$

Using these two bounds,

$$\mathbb{E}[|\bar{Y}_{\bar{\tau}} - Y_\tau|^2 \mid |\bar{\tau} - \tau| = s, \bar{\tau} \leq T] \leq c(\Delta + |\tau - \bar{\tau}|^2).$$

This gives that

$$\begin{aligned} \mathbb{E}[|\bar{Y}_{\bar{\tau}} - Y_\tau|^2 \mid \bar{\tau} \leq T] & \leq \int_0^T c(\Delta + |\tau - \bar{\tau}|^2) \Pr(|\bar{\tau} - \tau| = s \mid \bar{\tau} \leq T) ds \\ & \leq c \left(\Delta + \int_0^T s^2 \Pr(|\bar{\tau} - \tau| = s \mid \bar{\tau} \leq T) ds \right). \end{aligned}$$

Now we proceed to bound

$$\Pr(|\bar{\tau} - \tau| = s \mid \bar{\tau} \leq T) = \frac{\Pr(|\bar{\tau} - \tau| = s, \bar{\tau} \leq T)}{\Pr(\bar{\tau} \leq T)} \leq \frac{\Pr(|\bar{\tau} - \tau| = s)}{\Pr(\bar{\tau} \leq T)}.$$

Note that

$$\begin{aligned} \Pr(\bar{\tau} > T) &= \int_0^{T+1} \Pr(\bar{\tau} > T, \tau = s) ds \\ &= \int_0^{T-1} \Pr(\bar{\tau} > T, \tau = s) ds + \int_{T-1}^{T+1} \Pr(\bar{\tau} > T, \tau = s) ds \\ &\leq (T-1) \Pr(|\bar{\tau} - \tau| \geq 1) + \int_{T-1}^{\infty} \Pr(\tau = s) ds \\ &\leq (T-1) \mathbb{E}(|\bar{\tau} - \tau|) + (1 - F_\tau(T-1)) \\ &\leq c\Delta + (1 - F_\tau(T-1)), \end{aligned}$$

where F_τ denotes the CDF of τ . When T is properly large and Δ is small enough, we have $\Pr(\bar{\tau} > T) \leq 1/2$ and thus $\Pr(\bar{\tau} \leq T) = 1 - \Pr(\bar{\tau} > T) \geq 1/2$. This implies that

$$\Pr(|\bar{\tau} - \tau| = s \mid \bar{\tau} \leq T) \leq 2\Pr(|\bar{\tau} - \tau| = s).$$

We thus conclude that

$$\begin{aligned} &\int_0^T s^2 \Pr(|\bar{\tau} - \tau| = s \mid \bar{\tau} \leq T) ds \\ &\leq 2 \int_0^T s^2 \Pr(|\bar{\tau} - \tau| = s) ds \\ &\leq 2T \int_0^T s \Pr(|\bar{\tau} - \tau| = s) ds \\ &= 2T \mathbb{E}(|\bar{\tau} - \tau|) \\ &\leq c\Delta. \end{aligned}$$

We finally conclude that

$$\mathcal{W}^2[\bar{\pi}_T, \pi_T] \leq \mathbb{E}[|\bar{Z}_{\bar{\tau}} - Z_\tau|^2 \mid \bar{\tau} \leq T] \leq \mathbb{E}[|\bar{Y}_{\bar{\tau}} - Y_\tau|^2 \mid \bar{\tau} \leq T] \leq c\Delta.$$

□

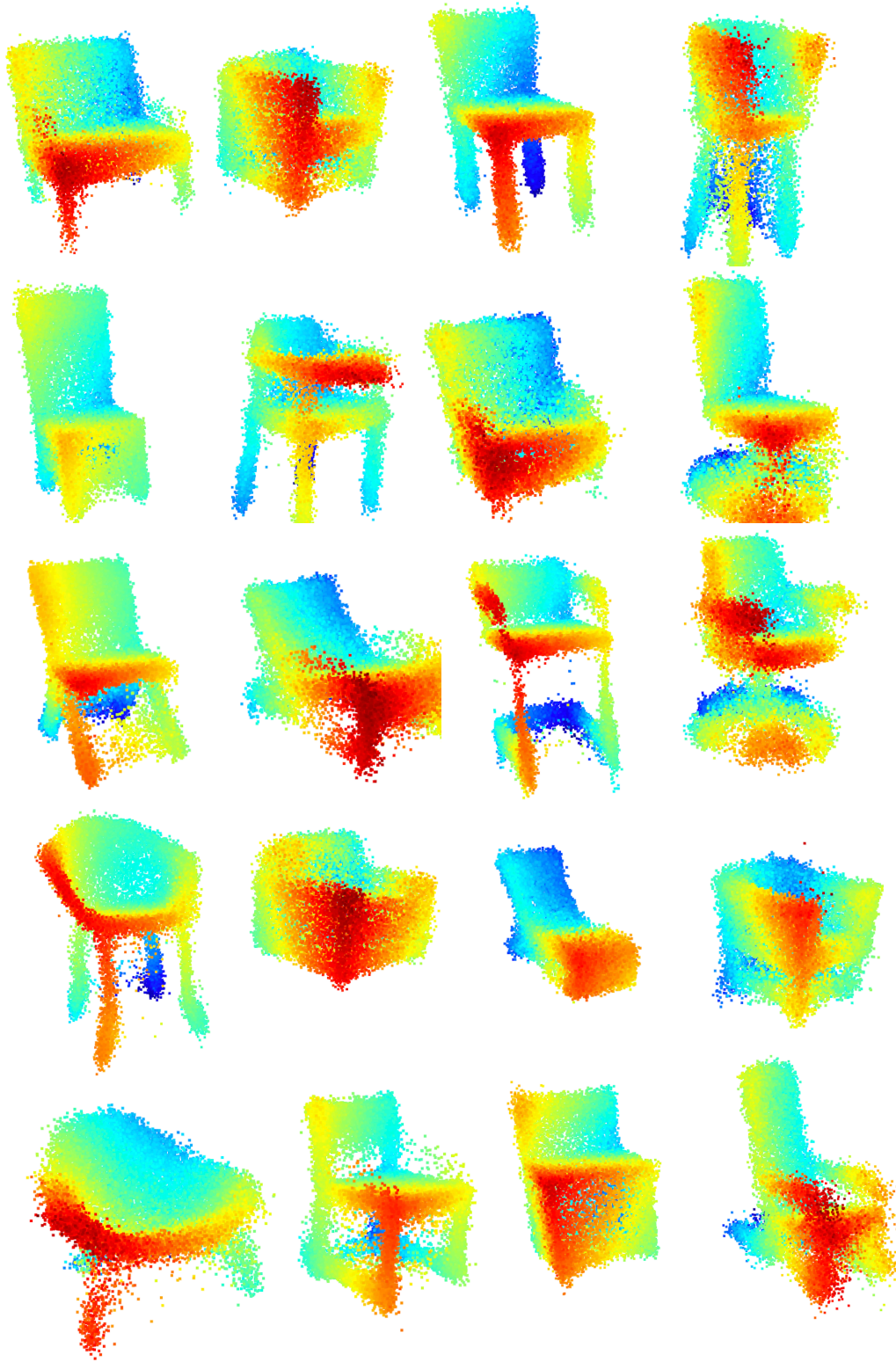
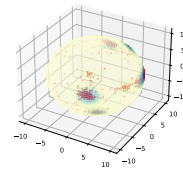
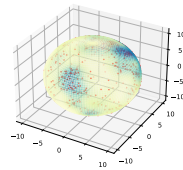
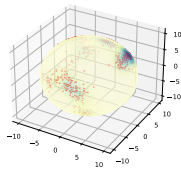
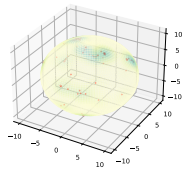
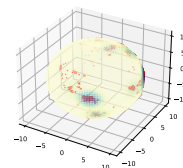
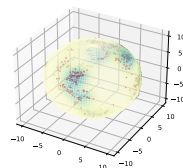
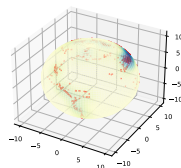
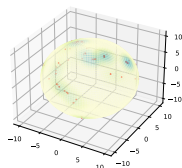


Figure 8: The generated chair point cloud by FHDM.

Generated



Data



Volcano

Earthquake

Flood

Fire

Figure 9: The generated distribution on sphere by FHDm.

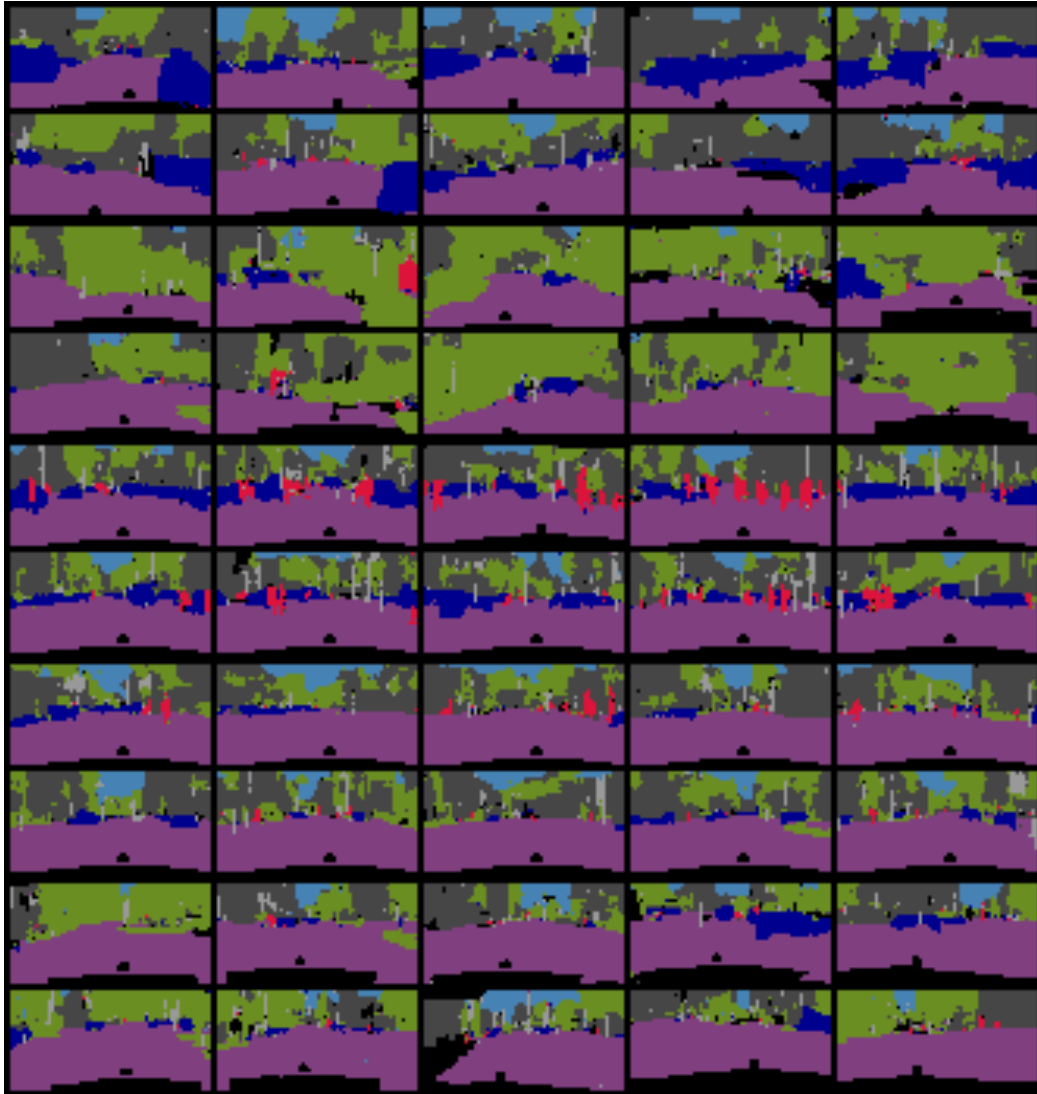


Figure 10: The generated segmentation maps by FHDM.

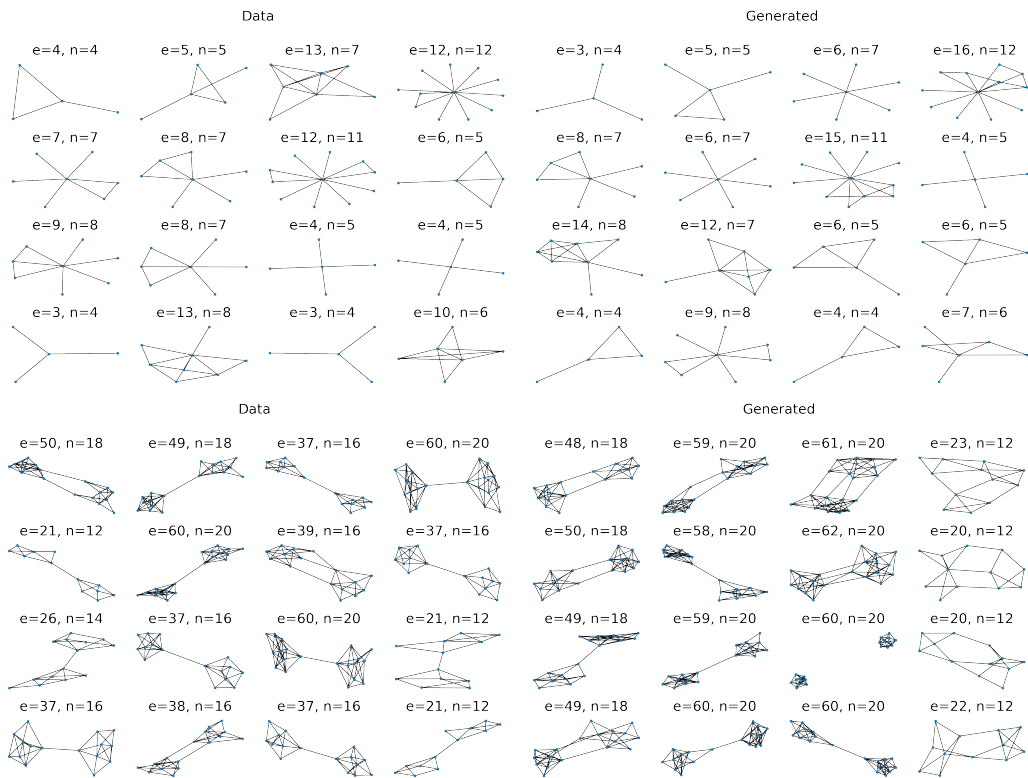


Figure 11: True and generated graphs of ego (upper rows) and community (lower rows) datasets.

A.9 Proofs

Proof of Proposition 2.3. As \mathbb{Q}^{B^d} is a product of identical and independent one-dimensional processes, it is sufficient to consider the one dimension case $d = 1$, in which case the process is a Brownian motion $dZ_t = dW_t$ starting from interval $Z_0 \in [0, 1]$ and stopped $\tau = \min_t\{t: Z_t \notin (0, 1)\}$ when it exits the interval. Hence, the Poisson kernel is

$$\mathbb{Q}_\Omega^{B^d}(x | z) = \Pr(W_\tau = x | W_t = z) = \Pr(W_\tau = x | W_t = z), \quad \forall x \in \{0, 1\}$$

Then, it is a textbook result that $\Pr(W_\tau = x | W_t = z) = xz + (1-x)(1-z) = \text{Ber}(x|z)$. See e.g., Eq. 3.0.4, Page 212 of Borodin and Salminen [3]. \square

Proof of Proposition 2.5. It is a straightforward application of formula (4) in the case of $b_t = 0$, $\sigma_t(Z_t) = \mathbb{I}(\|Z_t\| < 1)$ and $q_\Omega(x|z) = \frac{1-\|z\|^2}{\|x-z\|^d}$ as shown in (2). \square

Proof of Proposition 2.6. It is a straightforward application of formula (4) in the case of $b_t = 0$, $\sigma_t(Z_t) = \text{diag}(\mathbb{I}(Z_t \in (0, 1)))$ and $\mathbb{Q}_\Omega(x|z) = \text{Ber}(x|z)$ as shown in Proposition (2.3). \square

Proof of Proposition 2.7. This is the standard result on Brownian bridge. In particular, we just need to note that $(Z_T | Z_t = z) \sim \mathcal{N}(z, T - t)$ and apply formula (4). \square

Proof of Proposition 2.8. Eq. (13) is the direct result of $\mathbb{Q}^{\Pi^*} = \arg \min_{\mathbb{P}} \mathcal{KL}(\mathbb{P} || \mathbb{Q}^{\Pi^*})$, and that

$$\mathcal{KL}(\mathbb{P} || \mathbb{Q}^{\Pi^*}) \equiv \mathcal{KL}(\mathbb{P} || \mathbb{Q}) - \mathbb{E}_{\mathbb{P}}[\log \pi^*(Z_\tau)],$$

where we used $\mathbb{Q}^{\Pi^*}(dZ) = \mathbb{Q}(dZ)\pi^*(Z_\tau)$.

Eq (12) is a simple consequence of the disintegration theorem. Note that any \mathbb{P} that satisfies $\mathbb{P}_\Omega = \Pi^*$ can be written into $\mathbb{P}(dZ) = \Pi^*(dZ_\tau)\mathbb{P}(dZ | Z_\tau)$. By the chain rule of KL divergence,

$$\mathcal{KL}(\mathbb{P} || \mathbb{Q}) = \mathcal{KL}(\Pi^* || \mathbb{Q}_\Omega) + \mathbb{E}_{Z_\tau \sim \Pi^*} [\mathcal{KL}(\mathbb{P}(\cdot | Z_\tau) || \mathbb{Q}(\cdot | Z_\tau))]. \quad (20)$$

Since it is constrained that $\mathbb{P}_\Omega = \Pi^*$, the optimal \mathbb{P} is determined by the choice of $\mathbb{P}(\cdot | Z_\tau)$ and it should yield $\mathbb{P}(dZ | Z_\tau) = \mathbb{Q}(dZ | Z_\tau)$. Therefore, the optimal \mathbb{P} is $\Pi^*(Z_\tau)\mathbb{Q}(\cdot | Z_\tau) = \mathbb{Q}^{\Pi^*}$.

In fact, by the same derivation, we can see that (12) remains correct if we replace $\mathcal{KL}(\mathbb{P} || \mathbb{Q})$ with $\mathcal{KL}(\mathbb{Q} || \mathbb{P})$. \square

Proof of Proposition 2.9. Denote by $\mathbb{Q}^x = \mathbb{Q}(\cdot | Z_\tau = x)$. Let p^θ be the density function of \mathbb{P}^θ w.r.t. to some reference measure (e.g., \mathbb{Q}^{Π^*}). We have

$$\begin{aligned} \mathcal{KL}(\mathbb{Q}^{\Pi^*} || \mathbb{P}^\theta) &= -\mathbb{E}_{Z \sim \mathbb{Q}^{\Pi^*}} [\log p^\theta(Z)] + \text{const} \\ &= -\mathbb{E}_{x \sim \Pi^*} \mathbb{E}_{Z \sim \mathbb{Q}^x} [\log p^\theta(Z)] + \text{const} \\ &= \mathbb{E}_{x \sim \Pi^*} [\mathcal{KL}(\mathbb{Q}^x || \mathbb{P}^\theta)] + \text{const}, \end{aligned}$$

where $\mathcal{KL}(\mathbb{Q}^x || \mathbb{P}^\theta)$ can be evaluated using Girsanov theorem,

$$\begin{aligned} \mathcal{KL}(\mathbb{Q}^x || \mathbb{P}^\theta) &= \mathcal{KL}(\mathbb{Q}_0^x || \mathbb{P}_0^\theta) + \frac{1}{2} \mathbb{E}_{Z \sim \mathbb{Q}^x} \left[\int_0^\tau \|s_t^\theta(Z_t) - b_t(Z_t|x)\|_2^2 dt \right] \\ &= \mathbb{E}_{Z \sim \mathbb{Q}^x} \left[-\log p_0^\theta(Z_0) + \frac{1}{2} \int_0^\tau \|s_t^\theta(Z_t) - b_t(Z_t|x)\|_2^2 dt \right] + \text{const}. \end{aligned}$$

Hence

$$\begin{aligned} \mathcal{L}(\theta) &= \mathbb{E}_{x \sim \Pi^*, Z \sim \mathbb{Q}^x} \left[-\log p_0^\theta(Z_0) + \frac{1}{2} \int_0^\tau \|s_t^\theta(Z_t) - b_t(Z_t|x)\|_2^2 dt \right] + \text{const} \\ &= \mathbb{E}_{Z \sim \mathbb{Q}^{\Pi^*}} \left[-\log p_0^\theta(Z_0) + \frac{1}{2} \int_0^\tau \|s_t^\theta(Z_t) - b_t(Z_t|Z_\tau)\|_2^2 dt \right] + \text{const}. \end{aligned}$$

\square

Proof of Proposition 2.10. Assume $\|f\|_\infty := \sup_{t \in [0, +\infty), x \in [0, 1]^d} \|f_t(x)\|_2 < +\infty$. Consider the following two processes with the same initialization:

$$\begin{aligned} \mathbb{Q}^0: dZ_t &= \mathbb{I}(Z_t \in (0, 1)) \circ (\nabla_z \log \text{Ber}(\Omega | Z_t) dt + dW_t) \\ \mathbb{Q}^f: dZ_t &= \mathbb{I}(Z_t \in (0, 1)) \circ (f_t^0(Z_t) + \nabla_z \log \text{Ber}(\Omega | Z_t) dt + dW_t). \end{aligned} \quad (21)$$

Girsanov theorem shows that $\mathcal{KL}(\mathbb{Q}^0 || \mathbb{Q}^f) = \frac{1}{2} \mathbb{E}_{\mathbb{Q}^0} [\int_0^\tau \|f_t(Z_t)\|^2] \leq \frac{1}{2} \|f\|_\infty^2 \mathbb{E}_{\mathbb{Q}^0} [\tau] < +\infty$, where we used the fact that the expected hitting time $\mathbb{E}_{\mathbb{Q}^0} [\tau]$ of \mathbb{Q}^0 is finite (see Lemma A.1 below).

Now $\mathcal{KL}(\mathbb{Q}^0 || \mathbb{Q}^f) < +\infty$ implies that that \mathbb{Q}^0 and \mathbb{Q}^f has the same support. Hence the fact that \mathbb{Q}^0 guarantees to hit Ω when exiting V , i.e., $\mathbb{Q}^0(Z_\tau \in \Omega) = 1$, when exit implies that \mathbb{Q}^f has the same property, i.e., $\mathbb{Q}^f(Z_\tau \in \Omega) = 1$.

Lemma A.1. *Let $\tau^0 = \inf\{t: Z_t \in \Omega\}$ be the first hitting time to $\Omega \subseteq \{0, 1\}^d$ of the process \mathbb{Q}^0 in Eq. (21). Then $\mathbb{E}[\tau^0] < +\infty$.*

Proof. Consider the following two processes starting from the same deterministic initialization $Z_0 = Y_0 = z_0 \in (0, 1)^d$:

$$\begin{aligned} \mathbb{Q}^0: dZ_t &= \mathbb{I}(Z_t \in (0, 1)) \circ (\nabla_z \log \text{Ber}(\Omega | Z_t) dt + dW_t) \\ \mathbb{Q}^*: dY_t &= \mathbb{I}(Y_t \in (0, 1)) \circ (dW_t). \end{aligned}$$

Denote by τ^0 and τ^* the corresponding hitting times to Ω , that is, $\tau^0 = \inf\{t: Z_t \in \Omega\}$, and $\tau^* = \inf\{t: Y_t \in \Omega\}$.

Then we know from h -transform that \mathbb{Q}^0 is the conditioned process of \mathbb{Q}^* given that $Z_\tau \in \Omega$, that is, $\mathbb{Q}^0 = \mathbb{Q}^*(\cdot | Z_\tau \in \Omega)$.

Therefore, the first hitting time τ^0 of \mathbb{Q}^0 has the same law as that of $\tau^* | Y_\tau \in \Omega$, that is, $\mathbb{Q}^0(\tau^0 \in A) = \mathbb{Q}^*(\tau^* \in A | Y_\tau \in \Omega)$ for any measurable set $A \subseteq [0, +\infty)$.

But we know that $\mathbb{E}[\tau^* | Y_\tau \in \Omega] < +\infty$ due to the diffusion nature of Brownian motion. Hence, $\mathbb{E}[\tau^0] = \mathbb{E}[\tau^* | Y_\tau \in \Omega] < +\infty$. \square

\square

A.10 More Discussions on First Hitting Diffusion Models on \mathbb{R}^d

Assume the distribution Π^* of interest is on \mathbb{R}^d . To design first hitting diffusion models that yield results on Π^* , we embed \mathbb{R}^d into the hyperplane $\Omega := \{(x, y) \in \mathbb{R}^{d+1}: y = y_{\max}\}$ in \mathbb{R}^{d+1} where y_{\max} is a constant (e.g., $y_{\max} = 1$). We construct a baseline process $\bar{\mathbb{Q}}$ to be a diffusion process on \mathbb{R}^{d+1} :

$$\bar{\mathbb{Q}}: dZ_t = dW_t, \quad dY_t = b(Y_t, t)dt + \sigma d\tilde{W}_t, \quad Z_0 = z_0 \in \mathbb{R}^d, \quad Y_0 = 0, \quad (22)$$

where W_t and \tilde{W}_t are independent Brownian motions in \mathbb{R}^d and \mathbb{R} , respectively.

We can think Y_t as an ‘‘effective age’’ of the particle Z_t , and the sample is collected when $Y_t = y_{\max}$. Therefore, the hitting time of interest is $\tau := \{t: (X_t, Y_t) \in \Omega\} = \{t: Y_t = y_{\max}\}$.

A special case is $\sigma = 0$ and $b(Y_t, t) = 1$, in which case (Z_t, Y_t) hits the target domain Ω in the fixed time $t = y_{\max}$. This corresponds to the standard denoising diffusion models [e.g., 43].

Another extreme case is to take $b = 0$, so that Y_t is a Brownian motion without a drift. In this case, the hitting time follows an inverse Gamma distribution, and the exit distribution is a Cauchy distribution:

$$(\tau | Z_t, Y_t) \sim \text{InvGamma}\left(\frac{1}{2}, \frac{(y_{\max} - Y_t)^2}{2\sigma^2}\right), \quad (Z_\tau | Z_t, Y_t) \sim \text{Cauchy}\left(Z_t, \frac{y_{\max} - Y_t}{2}\right),$$

where the density of $\text{InvGamma}(\alpha, \beta)$ is $f(x; \alpha, \beta) = \frac{\beta^\alpha}{\Gamma(\alpha)} x^{-(\alpha+1)} \exp(-\beta/x)$, and density of $\text{Cauchy}(\mu, s)$ is $f(x; \mu, s) \propto (s^2 + \|x - \mu\|^2)^{-(d+1)/2}$.

An advantage of using random hitting is that it allows us to spend less time on generating Z_t that is close to the starting point (i.e., small $\|Z_t - x_0\|$), and more time on the further points. It allows us to adapt the time based on the ‘‘hardness’’ of the target distribution.

Accelerating the First Hitting Time The inverse Gamma distribution above has a heavy tail and occasional causes large hitting time. One way to ensure a bounded hitting time is to derive the conditioned process of Brownian motion given that the hitting time τ is no larger than a threshold. Specifically, assume $\mathbb{B} : dY_t = dW_t$ starting from $Y_0 = y_0 < y_{\max}$ and $\tau = \inf\{t : Y_t = y_{\max}\}$. Using h -transform, we can show that $\mathbb{B}(\cdot | \tau \leq T)$ is governed by the following diffusion process:

$$\mathbb{B}^T := \mathbb{B}(\cdot | \tau \leq T) : \quad dY_t = \nabla_y \log \left(1 - F \left(\frac{|y_{\max} - Y_t|}{\sigma \sqrt{T-t}} \right) \right) dt + \sigma d\tilde{W}_t,$$

where F is the CDF of standard Gaussian distribution.

Taking $b(Y_t, t) = \nabla_y \log \left(1 - F \left(\frac{|y_{\max} - Y_t|}{\sigma \sqrt{T-t}} \right) \right)$ in Eq. 22, we can obtain the following Poisson kernel for $\bar{\mathbb{Q}}$:

$$\bar{\mathbb{Q}}(Z_\tau = dx' | Z_t = x, Y_t = y) = \Gamma \left(\alpha, \frac{\phi(x'; x, y)}{T-t} \right) \frac{|y_{\max} - Y_t|}{\phi(x'; x, y)^\alpha} dx',$$

where $\alpha = \frac{d+1}{2}$ and $\phi(x'; x, y) = \frac{1}{2}((y_{\max} - y)^2 + \|x' - x\|^2)$, and $\Gamma(\alpha, x)$ is the upper incomplete gamma function. Correspondingly, the hitting time of this new process is $\text{InvGamma} \left(\frac{1}{2}, \frac{(y_{\max} - Y_t)^2}{2\sigma^2} \right)$ truncated on $[0, T]$.